STATIC AND DYNAMIC CHARACTERIZATION OF THE LIGAMENT SUBJECTED TO ALTERNATIVE WOUND HEALING

A Thesis

Presented to

the Faculty of the Department of Mechanical Engineering

University of Houston

In Partial Fulfillment

of the Requirements for the Degree

Master of Science

in Aerospace Engineering

by

Tripura Yelamarthi

May 2012

ACKNOWLEDGEMENTS

I dedicate my thesis to our beloved late Prof. David Zimmerman. Though he is physically absent, his suggestions and advice always guides me in each and every step of my life. I am very grateful to him.

I also owe gratitude to Dr. Daniel Martinez for his continuous support all throughout my research. His recommendations and critiques are key things that kept me moving in my research. In addition, I would like to thank Dr. Catherine Ambrose for providing me with precious information during experiments and analysis. I am grateful to Prof. Karolos Grigoriadis for all his support in the peak time. I thank Dr. Yi-Chao Chen for agreeing to be on committee on a short notice. I am thankful to Dr. Gangbing Song for lending the nano laser sensor for our experiments.

I am thankful to Gene Webster and Jerry Clifton for their support in the construction of the experimental setup. I would also like to thank the Mechanical Department Professors, staff and students for lending a hand and providing moral support when I needed it the most. Lastly, I thank all my friends and family members for endless support they rendered.

STATIC AND DYNAMIC CHARACTERIZATION OF THE LIGAMENT SUBJECTED TO ALTERNATIVE WOUND HEALING

An Abstract

of a

Thesis

Presented to

the Faculty of the Department of Mechanical Engineering

University of Houston

In Partial Fulfillment

of the Requirements for the Degree

Master of Science

in Aerospace Engineering

by

Tripura Yelamarthi

May 2012

ABSTRACT

The purpose of this study is to test the biomechanical properties of the rat (Rattus norvegicus) medial collateral ligament (MCL) following knee surgery and healing with the aid of Insulin-like growth factor (IGF-1) gene therapy treatments. The research work consisted of three stages: First, the design of a novel de novo technique that captures both static and dynamic characteristics of the knee ligament. Second, validation tests of this experimental apparatus were performed to show the repeatability of the measurements. Third, we measured the static characteristics, such as stiffness and strength and the dynamic characteristics, such as frequency and operating deflection shapes, of newly healed ligaments. Based on our analysis, surgically disrupted ligaments treated with the scAAV2-IGF-1b gene therapy treatment for three weeks displayed increases in ligament strength and toughness, suggesting that IGF-1b gene therapy may be a viable post-surgical treatment countermeasure for ligament repair.

TABLE OF CONTENTS

LIST OF FIGURES

LIST OF TABLES

CHAPTER 1

INTRODUCTION

Ligaments are collagenous tissues made up of collagen fibers and elastin fibers. The purpose of ligaments is to stabilize the joints by preventing them from excessive motion. The presence of the percentage of collagen and elastin fibers differs from ligament to ligament depending on the function of the ligament (Nordin and Frankel 2001). Knee joint ligaments are extensively studied due to the joint's elevated exposure to ligamentous stretches during daily physical activity and ligament injuries during professional sports (De Vita and Slaughter 2007; Panjabi et al. 1999). The knee joint consists of four ligaments, Medial Collateral Ligament (MCL), Lateral Collateral Ligament (LCL), Anterior Cruciate Ligament (ACL), and Posterior Cruciate Ligament (PCL). Medial collateral ligaments (MCL) along with anterior cruciate ligaments (ACL) are the most prone to injuries. Ligament injuries are classified into three degrees of sprains based on their severity (De Vita and Slaughter 2007). Of all musculoskeletal injuries, the highest annual occurrence with an average of 14.6 million in the years 1985-88 is seen in joint sprains with sub-failure ligament injuries (Panjabi et al. 1999). The present study is focused on acute MCL healing, novel gene therapy treatments and biomechanical testing.

The healing of the MCL as a function of the various treatments has been studied in animal studies (Provenzano et al. 2007; Gijssen et al. 2004). Various experimental models have been used to study acute dense fibrous connective tissue extracellular matrix healing during normal loading and periods of unloading (Provenzano et al. 2003; Provenzano et al. 2007).

Healing animals received different dosage of growth factors and/or growth promoting hormones. These treatments help to improve the speed and quality of healing to effectively reduce the rehabilitation times. Results from previous work illustrate that addition of GH alone did not have any significant effect while addition of IGF-1, GH+IGF-1 significantly improved biomechanical force, stress, and modulus values of healing MCLs and thus improved healing in collagenous tissue (Provenzano et al. 2007).

Experimental apparati such as, Varus Valgus (V-V) laxity device, Instron machine, MTS testing machines have been developed to evaluate and compare the function of the healing MCL with regard to joint stability as well as mechanical properties quantitatively (Woo et al. 1987; Vanderby et al. 1990; Paschos et al. 2010).

1.1 LITERATURE REVIEW

This section briefly discusses some of the publications representing the major approaches for acute ligament healing and experimental setups to analyze the various mechanical properties of tissues during the various phases of wound healing. Previously mechanical testing has been concentrated on determining static characteristics of ligament while the recent work also focuses on dynamic characteristics of biological tissues (Whittemore et al. 2004; Foth et al. 1996; Revel, Scalise, and Scalise 2003; Wang et al. 2007). Static characteristics are related to properties such as stiffness and load vs. deformation curves. Dynamic characteristics are related to vibrational/modal analysis such as natural frequencies, mode shapes and operation deflection shape.

Growth factors play a vital role in ligament healing. Growth factors increase the healing efficiency of ligaments by modulating the cell ability to up regulate the collagen synthesis. Collagens are group of proteins which are major structural elements of

connective tissues (Gelse 2003; Letson and Dahners 1994). Growth factors, namely, platlet-derived growth factor-BB (PDGF-BB), Insulin-Like Growth Factor-I (IGF-I), Transforming Growth Factor β (TGFβ), Vascular Endothelial Growth Factor (VEGF), Basic Fibroblast Growth Factor (bFGF), Growth and Differentiation Factor-5 (GDF-5) have been used for ligament healing (Letson and Dahners 1994; Molloy, Wang, and Murrell 2003; Tashiro et al. 2006). Ligament healing is further studied to investigate the effects of various growth factors during multiple stages of wound healing. Timothy et al studied the roles of five growth factors Insulin-Like Growth Factor-I (IGF-I), Transforming Growth Factor β (TGFβ), Vascular Endothelial Growth Factor (VEGF), Platelet-Derived Growth Factor (PDGF), Basic Fibroblast Growth Factor (bFGF) during tendon and ligament healing process. Results from this study conclude that IGF-I plays vital role during the inflammation and proliferation phase by promoting the proliferation and migration of cells, stimulating matrix production. TGFβ regulates cell migration and is most active during inflammation phase, whereas; VEGF, PDGF, bFGF are active during the proliferation and remodeling phase (Molloy, Wang, and Murrell 2003). Kurtz et al. studied effects of IGF-I on Achilles tendon healing. Results conclude that IGF-I is a major mediator in all stages of wound healing and significantly reduces functional deficit and accelerates functional recovery with no apparent loss to biomechanical properties (Kurtz et al. 1999). Earlier research work focused on the effect of IGF-I in animal studies. A limited amount of research has investigated the impact of IGF-1 as a treatment modality for acute ligament tears. Provenzano et al. studied systematic administration of IGF-I in rats with surgically disrupted MCLs and the results conclude that IGF-I significantly improved the MCL maximum force, ultimate stress, with significant

increases in matrix organization and type-I collagen expression (Provenzano et al. 2007). Recently, Hansen et al. studied the local administration of IGF-I in human tendon tissues and the results show that IGF-I directly enhances the tendon collagen synthesis both within and around the human patellar tendon tissue (Hansen et al. 2012).

Healing of ligaments has been studied under conditions such as loading, unloading, mobility and immobility in rats. The results show that early motion and exercise of ligament results in increased strength compared to stabilized ligaments (Lechner and Dahners 1991; Provenzano et al. 2003). Healed ligaments are assessed by measuring various factors such as tensile strength, stiffness, stress at failure, maximum load to failure using mechanical testing machines (Hart and Dahners 1987). Some of the earliest work in rapid ligament healing demonstrated static characteristics such as stress-strain relationships to determine ligament strength by various approaches. An example of such devices are; A laxity device was designed to test the knee in tension to determine the structural properties of femur-MCL-tibia complex (FMTC) and mechanical properties of the healing MCL substance (Woo et al. 1987). The FMT specimens were gripped with specially designed fixtures and inserted into a MTS testing machine (Model T5001, Minnetonka, Minn.) for biomechanical testing. Tangent modulus, ligament stretch at failure, ligament stress at failure, ultimate load of FMT and ultimate load are found using this test machine (Vanderby et al. 1990). FMT specimens were submerged in a cylindrical Plexiglas tank containing physiological buffer and a tensile test was performed to study the mechanical properties of ligament after hind limb suspension (Vailas et al. 1990). Past work on static characteristics used large testing machines such as laxity devices, MTS machine, MTS actuator, LVDT machines and strain-gauge to

determine parameters tensile strength, area, and ultimate load (Hart and Dahners 1987; Gijssen et al. 2004; Vanderby et al. 1990; Woo et al. 1987). Static characteristics are further studied using test machines composed of a load cell and picomotor. Specifications related to maximum load capacity of cell and displacement rates of picomotor have widely varied. Warden et al. performed experiments with 50N and 22N load cells and displacement rates 0.5 mm/s and 0.3 mm/s. The replacement of load cell resulted in force and displacement resolution of 0.001 N and 0.001 mm respectively. Selection of picomotor and load cell is based on the resolution, accuracy, maximum load required for the test and length of specimen. Higher resolution and accuracy have been obtained with the use of optimized equipment (Warden et al. 2006). Paschos et al. performed research on anterior cruciate ligament with load cell and displacement rates 5 kN and 1.5 mm/s respectively (Paschos et al. 2010). Nishimori et al. conducted a research on injured MCL with a displacement rate 0.25 mm/sec (Nishimori et al. 2012). In all these studies, mechanical properties of ligaments and tendons were determined by evaluating static characteristics such as stiffness and load to failure. Revel et al. presented a new non-intrusive experimental procedure to determine mechanical properties of tendons based on the dynamic characteristics such as resonance frequency measured by Laser Doppler Vibrometer (LDV). For each loading condition, vibration resonance frequency and tensile force were measured. Stress- strain curves were correlated with first resonance frequency recorded by the LDV to determine relation of stress and strain with resonance frequency. Research was performed *in vitro* with an aim to establish a mechanical procedure which could also be used for *in vivo* experiments (Revel, Scalise, and Scalise 2003).

Dynamic characteristics, such as natural frequencies, resonance frequency, mode shapes and modal analysis are related to the field of vibration testing. Vibration testing is study of vibrations, with many engineering applications, such as, the design of machines, structures, foundations, turbines, steam and gas engines, space systems and satellites. In all these applications, structure or machine components can fail because of material fatigue resulting from induced stress from cyclic vibrations. When the natural frequency of vibration of a machine or a component coincide with the frequency of the external excitation, a phenomena called resonance occurs, which leads to excessive deflections and potential failures. To assess the effects caused by vibrations, vibration testing is a standard procedure in the design and development of structural engineering systems (Rao 2006). During vibration testing, natural frequencies of structures are determined to perform structure modification and design optimized structures. Zhao et al. performed vibration testing on solar panels using LDV. The results helped in designing an optimized solar panel by providing physical and structural parameters with desired structural properties (Zhao et al. 2011). Laser vibration sensing also has found applications in defense and security in the detection of land mines, camouflaged or concealed targets (Scalise et al. 2011). Similarly, the study of the dynamic characteristics of biological tissues originated to determine mechanical properties, such as, stiffness and movement of tissues using natural frequencies and mode shapes.

Previously, dynamic characteristics were evaluated in biological tissues using vibrators and accelerators. Wang et al. measured dynamic characteristics in patellar tendon, a soft tissue of the human body. An electric vibrator was used to transmit vibrations into the tibia and patellar tendon. An accelerometer was attached to the

vibrator to determine the energy delivered to tissue. A second accelerometer was attached to patellar tendon to record the vibration of the patellar tendon. Results established that resonance frequencies exist in soft tissues and this characteristic is useful in detecting changes in the tissues (Wang et al. 2007). Resonance frequencies of goat vertebral motion segments have been studied using a shaker attached to upper vertebra and a response was obtained from accelerometers on the anterior side of upper vertebra. This study determined that structural changes such as mass and stiffness could be determined by recorded resonance frequencies (Van Engelen et al. 2011). Christensen et al. studied resonance frequencies and mode shapes for the assessment of tibial stiffness in human body. Resonances were measured by impedance probe technique where the leg was placed in a specially developed splint. The results provide the mechanical stiffness of the tibia and the sensitivity of these measurements to the soft tissues present around the tibia (Christensen et al. 1986; P. Cornelissen et al. 1986; M. Cornelissen et al. 1987).

In the present research work, an LDV approach was used for determining the dynamic characteristics of biological tissues. Laser Doppler vibrometry has been used in the field of otology to determine parameters in reconstructed ears, by measuring the tiny motions caused by the tympanic membrane in human along with an assessment of errors occurred during the measurements (Whittemore et al. 2004; Foth et al. 1996; Sim et al. 2010; Eiber 2008). LDV has also been used for dynamic characterization of the middle ear model. Detected vibrations of the middle ear ossicles showed regular and irregular behavior in presence of any damage (Rusinek et al. 2011; Zhang et al. 2007). Castellini et al. studied teeth mobility with the application of dynamic loads for *in vitro, in vivo* cases using LDV to determine the stiffness of the support, one of the parameters for teeth

mobility. Results establish that with this new technique tooth mobility could be determined before it becomes evident and problematic (Castellini, Scalise, and Tomasini 1998). Lorenzo et al. evaluated measurement of respiration rate in preterm infants using LDV. This was assessed by the detection of abdominal walls movement by LDV which was operated at a distance from patient and outside the incubator (Scalise et al. 2011). Thus measurement of vibrations and dynamic characteristics using LDV has made its place even in the field of biology.

Likewise dynamic characteristics of ligaments can be measured using LDV. Resonance frequency is related to the stiffness of ligament and mode shapes represent the sequence of motion of elements in ligaments. A similar test machine was built by Revel et al. for tendons as shown in Figure 1.1.

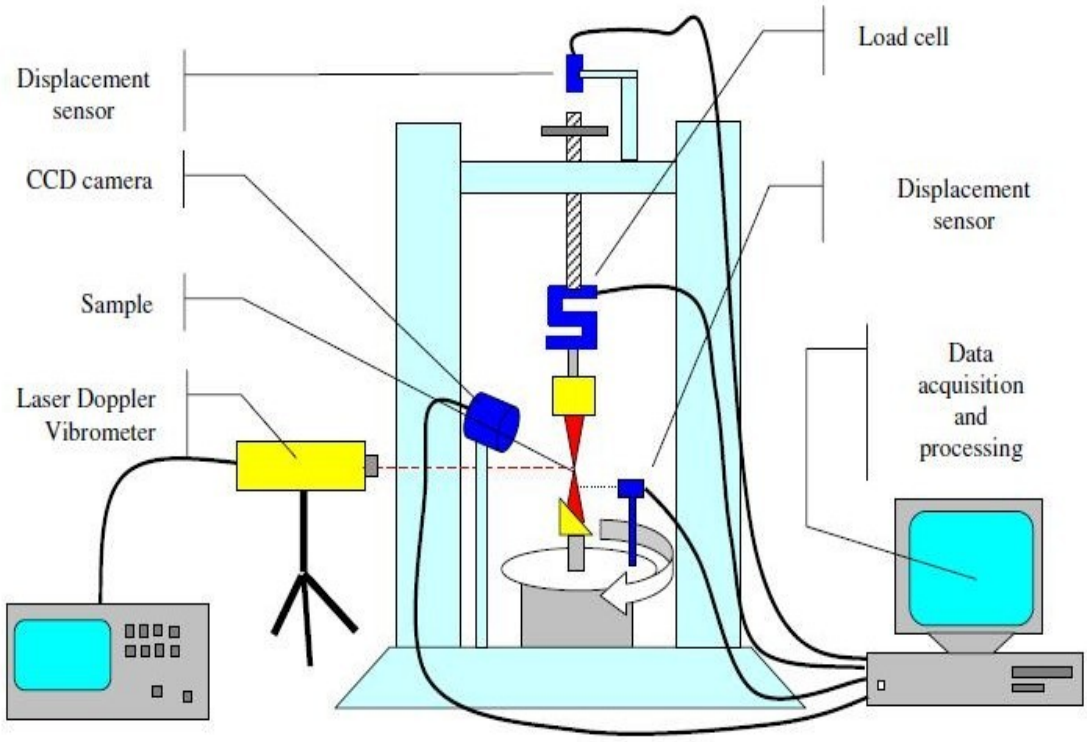

Figure 1. 1 Test machine built to evaluate resonance frequencies and determine mechanical properties of tendons (Source: Revel et al., 2003)

Previous work related to construction of a mechanical test machine was focused on either determining static characteristics or dynamic characteristics of ligaments. Motivated by previous work, this thesis proposes to use an experimental apparatus in which both static characteristics and dynamic characteristics will be simultaneously measured in Medial Collateral Ligaments (MCL) treated with IGF-I isoform gene therapy to improve ligament healing time.

1.2 SIGNIFICANCE

Inspired by previous work, an experimental apparatus was built in this project to determine both static and dynamic mechanical characteristics, of rapidly healing ligaments. The experimental apparatus was divided into two sections. One, a "custom-built" load frame to evaluate static characteristics such as stiffness and the load to failure of ligaments. Second, Laser Doppler vibrometry was used to estimate dynamic characteristics, such as, resonance frequencies and operating deflection shapes of ligaments.

It is hypothesized that this new apparatus can be used to measure the material properties of rodent MCLs. These ligaments were obtained from an *in vivo* experiment where injured ligaments were treated with IGF-1 gene therapy. For these treatments, autologous MCL fibroblasts were transfected with a novel non-pathogenic self-complementary adeno-associated virus that over expresses insulin like growth factor-1(scAAV-IGF-1) and were introduced into the wound area using Tissel fibrin glue as a vehicle (Martinez and Zimmerman 2008). Previous studies have demonstrated that insulin like growth factor-I (IGF-I) plays a crucial role in muscle generation, can reduce age-related loss of muscle function, and can cause muscle hypertrophy when over

expressed (Provenzano et al. 2007). In the present study, we test three IGF-I isoform gene therapy treatments in three groups of animals and compare the IGF-I gene therapy treatments to 1) a control gene therapy green fluorescent protein treatment group and 2) a non injured Sham control group receiving no treatment. The treatment groups are as follows: Sham Controls (n=6), scAAV2-GFP (n=6), scAAV2-IGF-1a (n=6), scAAV-2-IGF-1b (n=6) and scAAV2-IGF-1a + scAAV2-IGF-1b combination treatment (n=6). These treatment groups are discussed in further chapters.

CHAPTER 2

THEORY AND BACKGROUND WORK

2.1 BIOMEDICAL BACKGROUND

Three experimental approaches *ex vivo, in vitro* and *in vivo* were used to investigate the transduction of MCL derived cells with scAAV2-constructs within a Tissel™ Fibrin-glue delivery vehicle as depicted in Figure 2.1. In my thesis, I used the samples derived from the i*n vivo* research project to perform the biomechanical analysis. (A) In the *ex vivo* approach, MCL fibroblasts are harvested, grown to confluence and cryobanked in LN2 for future use. (B) Vials of 1 x 10^6 MCL fibroblasts were thawed and grown to 60 – 80 percent of confluence, transduced with the scAAV2 vector-construct of interest using the AdenoMag™ AAV magneto-transduction reagent and methodology to increase the transduction efficiency of the transgene by accelerating and concentrating the virus to the cell monolayer. (C) *In vitro* experiments were performed to characterize the behavior and function of the scAAV2-contructs after transduction. The characterizations include 1) scAAV2 cell titers, 2) cell number versus IGF-1 are measured using IGF-1 ELISA assays and 3) the optimization of the number of transduced cells (18.5K, 37.5K and 75K cells) compared to 50% and 75% Tissel™ fibrin glue concentrations. (D) In the *in vivo* animal experiments, 50% Tissel™ fibrin-glue plus 75,000 transduced scAAV2-constructs were used in all MCL surgical repairs.

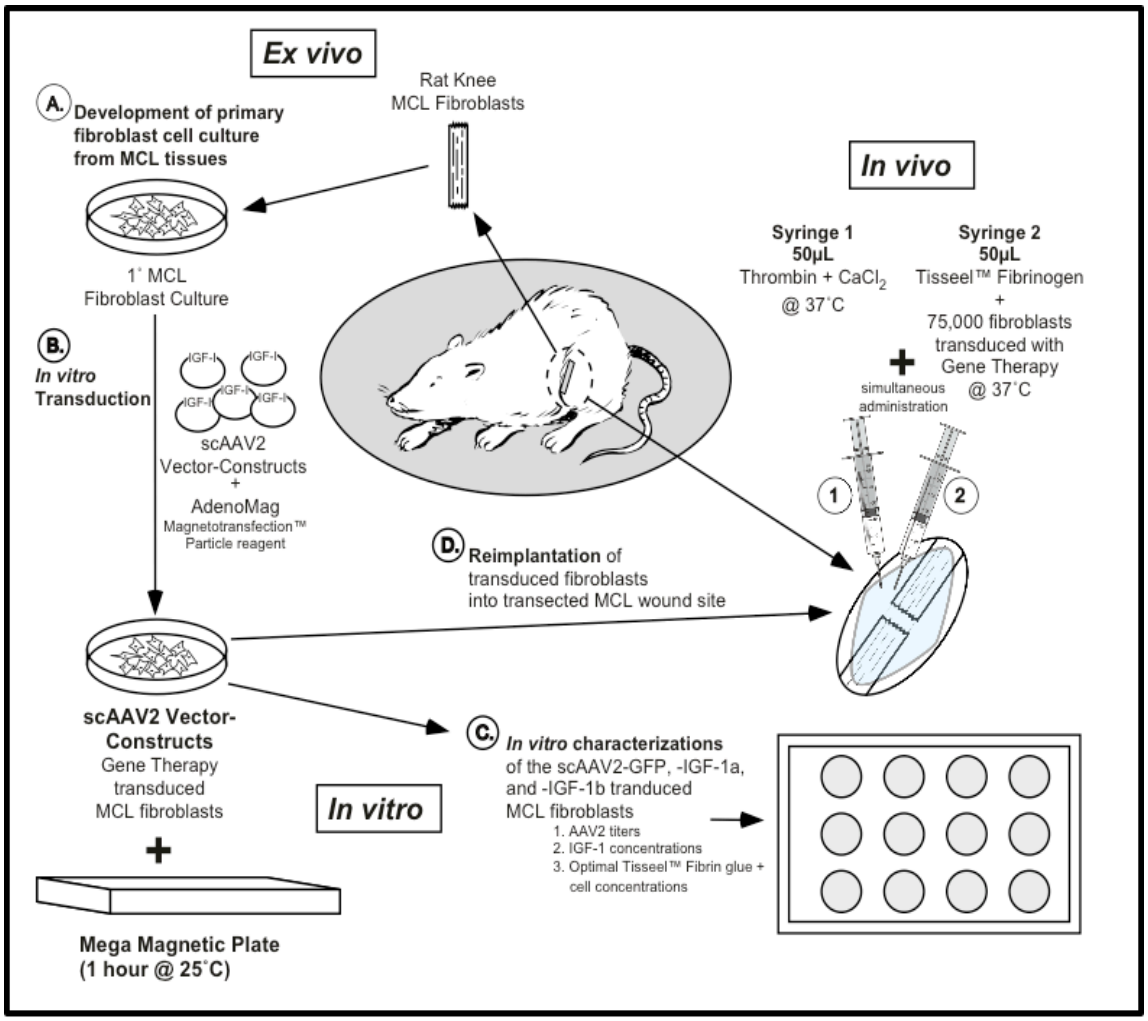

Figure 2. 1: A schematic illustration of ex vivo (indirect), in vitro studies, and in vivo (direct) gene therapy delivery paradigms that were employed

2.1.1 Animal Care

Male Sprague-Dawley rats were housed in a temperature controlled (23 ± 2ºC) room with a 12-hour light-dark cycle in an American Association for Accreditation of Laboratory Animal Care-accredited animal care facility and were provided standard rodent chow (Harlan Teklad 8604) and water ad-libitum. All animal care and experimental procedures described in this investigation were conducted in accordance with the University of Houston Laboratory Animal Care Committee regulations (09-021R).

2.1.2 Isolation of Primary Rat MCL Fibroblasts for *Ex Vivo, In Vitro and In Vivo* Experiments

Rats from Harlan Laboratories were received (n = 10), placed in vivarium cages, and allowed to adapt to their new environment for 7-10 days. The animals received water and food *ad libitum*. To isolate primary rat medial collateral ligament fibroblasts (MCL), the rats were euthanized via inhalation overdose of CO_2 gas and cervical dislocation to ensure animal euthanasia. Quickly, 3-2 – 4 MCLs were surgically harvested from the rat right and left knees, rinsed Hank's Balanced Salt Solution (HBSS) plus penicillin-streptomycin (P/S), minced with sterile mayo scissors and plated in complete 2 mL of DMEM/F-12 media containing 10% fetal bovine serum (FBS) and 1% P/S including 0.3% gentamicin. The propagated primary (1°) rat MCL fibroblasts were rinsed of tissue and cellular debris and fresh media was added every 3 – 4 days. The 1° rat MCL fibroblasts were passed into 75 cm^2 tissue culture flasks 1x to increase cell number, lifted, gently pelleted, mixed with 5% DMSO in complete media, slowly frozen in a gradient manner (24 hrs. at -85°C ethanol immersed cryo-vials containing 1 x 10^6 fibroblasts in a Nalgene LoBoy™ cryo-container) and finally stored in LN_2 for future *in vitro* and *in vivo* experimental protocols.

2.1.3 *In Vivo* Animals and Experimental Design

Forty-eight (48) male Sprague-Dawley rats were obtained from Harlan (Houston, TX) at 64 – 69 days of age and allowed to acclimate to their surroundings for 10 days prior to initiation of the study. Five experimental groups were used in the study:

1. Sham surgery control group (Sham, n = 9)
2. MCL surgically transected ligaments treated with scAAV2-GFP gene therapy

(GFP group, n = 10)

3. MCL surgically transected ligaments treated with scAAV2-IGF-1a gene therapy (IGF-1a group, n = 10)
4. MCL surgically transected ligaments treated with scAAV2-IGF-1b gene therapy (IGF-1b group, n = 10)
5. MCL surgically transected ligaments treated with a combination of scAAV2-IGF-1a + scAAV2-IGF-1b gene therapy (IGF-1a + IGF-1b group, n = 9)

2.1.4 *In Vivo* Animal Model and Surgical Procedures

Pre-Surgical Procedures

All surgical procedures were performed aseptically. The rats were anesthetized/ induced with 2-3% isoflurane inhalation using a nose cone and the hindlimbs and surrounding area were immediately shaved with a #50 Oster blade, swabbed with chlorohexidine, since the use of betadine to prevent infection is contraindicated with the use of Tissel™ fibrin glue.

Surgical Procedures

During the procedure the animals were continuously anesthetized to a level plane of anesthesia (1.5% - 3% isoflurane) and were monitored of the animal's respiration and other vital signs will be maintained. A small skin incision was made on the inner (medial) side of both knees. A surgically transected, rather than torn, medial collateral ligament (MCL) was used as the experimental model to create a uniform defect for healing. Rats were subjected to bilateral MCL transection using sterile techniques (n = 39 animals). A 1-cm skin incision was made over the medial aspect of each stifle, and the subcutaneous tissue was dissected to expose the sartorius muscle and underlying MCL. The midpoint of

the MCL was completely transected. Severed ends were not sutured and allowed to retract. A Sham group (n = 9) was created to control for the animal surgical process however the main difference was that the medial collateral ligament was exposed (Sham) and not surgically transected nor treated with gene therapy. The Sham group was used as a positive control group for the biomechanical bone-ligament-bone dynamic and static testing.

Application of Tissel Fibrin-glue and IGF-1 gene therapy

After the MCL was transected, a bilateral treatment at the wound site of Tissel fibrinogen™ (50%) mixed with 7.5 x 10^4 transduced primary MCL fibroblasts (50 µL aliquot per knee) mixed simultaneously with Thrombin-$CaCl_2$ (50 µL aliquot per knee) maintained at 37˚C in a heat block (1.5 mL conical tube holder, digital VWR electronic block heater) to form an opaque fibrin-glue plug matrix scaffold containing the gene therapy within 10-30 seconds after application. The underlying fascia and skeletal muscle was sutured with 2 – 3 simple interrupted surgeon's knots using 4.0 absorbable chromic gut suture materials (FS – 2, 19mm 3/8c – reverse cutting needle, Ethicon, Johnson & Johnson Endo-Surgery, Inc.). The skin incision was closed with 2 – 3 non-absorbable nylon simple interrupted sutures (FS – 2, 19mm 3/8c – reverse cutting needle, Ethilon, Ethicon, Johnson & Johnson Endo – Surgery, Inc.). During the surgery the bilateral procedure was accomplished in 30 – 40 minutes on average. Ten animals were subjected to bilateral MCL transection per day, 1 group per day and/or 5 groups of 10 over 5 days. For analgesia, the animals were given 5mg/mL of infant Tylenol analgesic in water maintained in each cage for 48 hours post-surgery. Following 48 hours, the animals were switched to pure drinking water for the remainder of the experiment.

Healing time-course and euthanasia

The animals were allowed to heal over a 21-day period to simulate an acute healing phase. Since the animals were staggered by groups over 5 days during the initial surgery, 10 animals per day after 21 days were anesthetized (1.5% - 3% isoflurane), exanguinated by cardiac puncture (3 – 5 cc of heparinized blood) to collect blood plasma to measure circulating levels of IGF-1 protein, then were subjected to cervical dislocation via a rodent guillotine. Final rat body weights ranged from 372±2 g to 383±7 g in animals ranging from 85 to 90 days old following 21 days of MCL healing. The following hindlimbs and MCL tissues were carefully dissected and distributed using the following schema as depicted in Table 2.1.

Table 2. 1: Treatment Groups

Groups	Left Leg
Sham Group (n = 9)	6 femur-MCL-tibia legs
scAAV2-GFP Group (n = 10)	6 femur-MCL-tibia legs
scAAV2-IGF-1a Group (n = 10)	6 femur-MCL-tibia legs
scAAV2-IGF-1b Group (n = 10)	6 femur-MCL-tibia legs
scAAV2-IGF-1a+IGF-1b Group (n = 10)	6 femur-MCL-tibia legs

2.1.5 Biomechanical Measurement of Femur-Ligament-Tibia Samples

The left hindlimb legs (n = 6) were dissected free from the pelvic girdle by freeing the femur head from the acetabular socket. The legs were dissected (50-75%) free of skeletal muscle and rinsed in sterile PBS, pH 7.4, and wrapped in gauze soaked in PBS, followed by plastic wrap, then wrapped in labeled foil and placed on dry ice followed by long term ultralow temperature storage (-85˚C). The samples were later

thawed 1x to remove the remaining skeletal muscle and soft tissue to expose the MCL for biomechanical testing. The samples were kept in a humid environment by applying droplets of PBS and re-wrapped in gauze soaked with PBS, wrapped in plastic and foil and re-frozen until dynamic and static biomechanical testing. [Material obtained from Dr. Daniel Martinez].

2.2 MECHANICAL CHARACTERISTICS

In biomechanical testing we determined the static and dynamic characteristics of the healing ligaments. The static characteristics measured were the mechanical properties of stiffness, maximum load to failure, energy necessary to break a ligament. Dynamic characteristics obtained were the natural frequencies and operating deflection shapes of the ligament.

2.2.1 Static Characteristics

All static characteristics were determined from the load-displacement curves generated using data recorded from load cell and nano laser displacement sensor.

Stiffness

To estimate stiffness, a basic straight line fit was evaluated for each load-displacement graph. Straight line fit estimates slope of the curves. This slope is generally known as structural stiffness (Gijssen et al. 2004). In this study, we refer to structural stiffness as: stiffness of the ligament.

Load to failure

The maximum (or ultimate) load was obtained from each load-displacement graph (Nordin and Frankel 2001).

Elastic Storage Energy and Work to Failure

In load-displacement curves, the area under the curve from start point to maximum load was evaluated. This area is the energy consumed by the ligament in the elastic region before it fails. It is known as elastic storage energy.

In the load-displacement curves, the total area under the curve from start point till complete failure of the ligament was also evaluated. The energy consumed by the ligament before it fails completely is related to the toughness of the ligament. It is also known as Work to Failure (Nordin and Frankel 2001).

In general the area under the curve is estimated by using an integral function. A definite integral function determines the area, under a curve with a known equation. The area under the curve was calculated using the trapezoidal rule. Trapezoidal rule is an approximate technique for calculating definite integral (Atkinson 1989),

$$\int_{a}^{b} f(x)dx \approx (b-a)\frac{f(a)+f(b)}{2}. \qquad \textit{equation 2. 1}$$

2.2.2 Dynamic Characteristics

Natural Frequency

The frequency at which a system oscillates when it is disturbed and allowed to vibrate on its own without any external forces or damping is known as Natural Frequency. It is denoted by ω_n. The natural frequency is a function of stiffness (k) and mass (m) of the system. It is directly proportional to the stiffness and inversely proportional to mass of the system (Rao 2006). In our tests we determine the natural frequency from the Frequency Response Functions (FRFs) and it is related to the stiffness of the ligament,

$$\omega_n = \sqrt{\frac{k}{m}}. \qquad \textit{equation 2. 2}$$

Resonance Frequency

When the natural frequency of a system coincides with the frequency of external excitation, a phenomenon known as resonance occurs. The frequency at which resonance occurs is known as Resonance Frequency (Rao 2006).

Frequency Response Function (FRF)

The function generated to express the response of a system when subjected to harmonic excitation is called Frequency Response Function (FRF). This function is defined over the range of frequencies applied to a system. Fast Fourier Transform (FFT) is used in the process of generating this function (Ewins 1984; Ewins 2001; Rao 2006).

Operating Deflection Shape (ODS)

The Operating Deflection Shape (ODS) defines the deflection of a structure at a particular frequency. It can also be defined as forced motion of two or more points of a structure. The values of a set of frequency domain responses at a specific frequency define the operating deflection shape (Schwarz and Richardson 1999). In our test we determine ODS of the ligament at detected natural frequencies.

Mode Shapes

Mode Shapes are obtained from operating deflection shapes. It is the sum of single degree freedom deflections in a decoupled system and is created by fitting the model of the system. In our tests we study operating deflection shapes. Operating deflection shapes are just values whereas; mode shapes are obtained/calculated from equation of the structure (He and Fu 2001).

Excitation

Resonance frequencies, frequency response functions and operating deflection shapes can be evaluated when a structure is vibrating under forced excitation. Excitation mechanisms are classified on the basis of attached and non-attached devices. A shaker is an attached device while an impactor is not (although it does make contact for a short period of time) (Broesch, Stranneby, and Walker 2008).

Impact excitation is a simpler technique to implement due to ease of setup, fast measurement acquisition time and relatively low cost of equipment, however, it is, difficult to obtain consistent results. The most commonly used impact device is a hammer (Broesch, Stranneby, and Walker 2008).

In shaker excitation, some prespecified or random excitation is given and the input signal and response signal are studied. Windowing may be used to minimize the data leakage. The input forces given to the shaker are generally classified into two categories - deterministic and random signals. Each of these signals is used to determine the characteristics of the system such as generation of frequency response function and linearity of system (Broesch, Stranneby, and Walker 2008). Types of these signals are studied in further chapters. Thus these excitation techniques are used to study the dynamic characteristics required for estimation of mechanical properties of ligament.

CHAPTER 3

PROCEDURE

3.1 EXPERIMENTAL APPARATUS

The apparatus consists of custom-built load frame and laser vibrometer. In the custom-built load frame, a picomotor is used to drive one axis of a three-axis stage. The picomotor is computer controlled to give forward or reverse movement. This is used to load and unload the ligament. The load is measured using a calibrated load cell. A laser displacement sensor reads the displacement of the stage. The laser vibrometer is used to detect the vibrations in the ligament. During the measurement of the dynamics, a small speaker excites the ligament acoustically.

3.1.1 Picomotor

Picomotor actuators are ideal devices for motorizing fine – positioning stages and mounts in any optical or mechanical systems. We use a Newport motorized SS Crossed - Roller 1 in. XYZ translation stage model 9067 – XYZ – NPN with motorized Y-axis and a manual X and Z-axis. In the motorized stage, the motorized axis is mounted with an 8303 picomotor while the rest of them are mounted with a 9353 micrometer. Picomotor has a travel range of 50.8 mm with a resolution < 30 nm. Maximum speed of picomotor is 1.2 mm/min. Maximum load capacity of picomotor is 22 N. The motorized stage is shown in Figure 3.1. In Figure 3.1 the red horizontal device is the picomotor, whereas the vertical silver device is the micrometer.

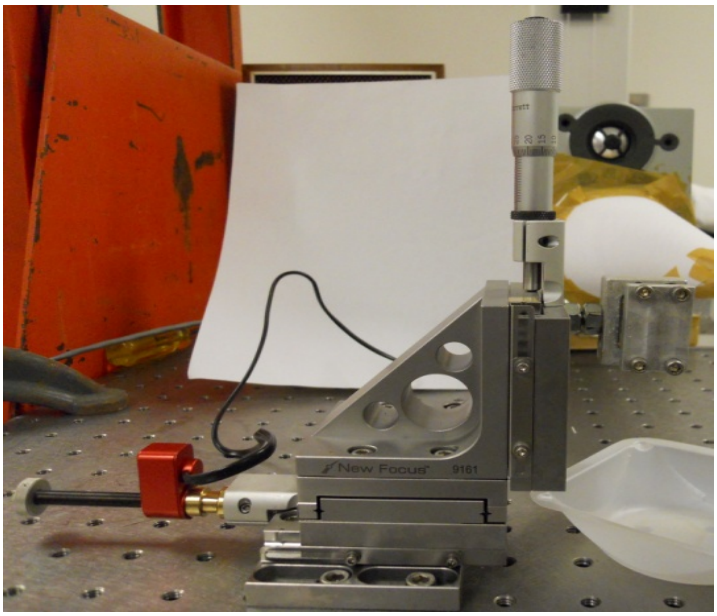

Figure 3. 1: Motorized stage with picomotor and micrometer

To drive and control the picomotor actuators a three – axis iPico driver kit of model 8763 – KIT is used. The kit is shown in Figure 3.2.The kit is equipped with a network controller and a driver for controlling up to three individual picomotor actuators. It includes a model 8752 Ethernet controller, a model 8755 power supply, and one model 8753 iPico driver. The kit is computer controlled by RS-232 and with the software program iPico MCL Control Panel by NEWFOCUS for the forward and reverse movement of the picomotor and also in the form of specified number of tics.

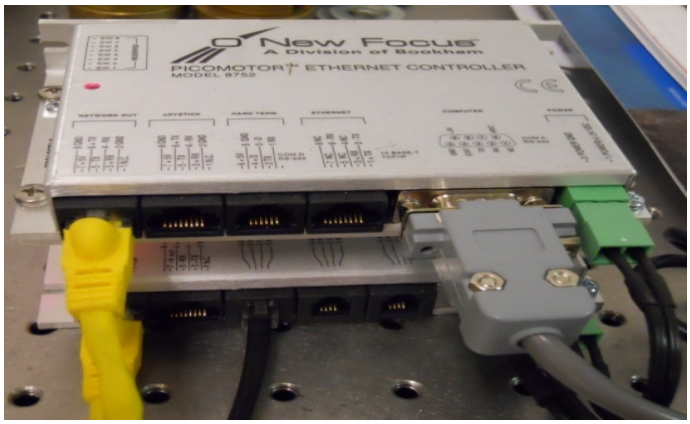

Figure 3. 2: Picomotor driver kit

3.1.2 Load cell

A load cell is a transducer that converts a load into an analog electrical signal. Strain gage type load cells are the commonly used type. In this through a mechanical arrangement the force is sensed, which deforms a strain gage. The strain gage converts the deformation into an electrical signal. We use Transducer Techniques Load Cell of MDB series and a display meter DPM-3. Maximum load capacity of load cell is 44.48 N (10 lbs). The load cell is shown in Figure 3.3.

Figure 3. 3: Load Cell

The DPM-3 converts the analog electrical signal to digital and displays the load read by the load cell. It has various settings such as decimal point, low signal input, desired reading at low input, high signal input, desired reading at high input, baud rate and output update rate. All these are set according to the requirement. It is scaled and set to read the load in pounds. The graphical programming software LABVIEW is used to interface with DPM-3 and collect the data from it and store it in excel sheets. The DPM-3 is shown in Figure 3.4.

Figure 3. 4: Display Meter DPM – 3

3.1.3 Laser Displacement Sensor

A CCD Displacement Laser Sensor is used to measure the displacement of the stage and thus that of the ligament. We use a Keyence Laser Displacement Sensor LK – G32 head and LK – GD500 controller. The laser displacement sensor is shown in Figure 3.5 whereas the controller is shown in Figure 3.6.

Figure 3. 5: Nano Laser Sensor

Figure 3. 6: Controller

The controller has various settings related to scaling, tolerance, decimal point, trigger, filter, sampling rate etc. The controller has two displays OUT1 and OUT2. Both of them can be configured as needed and that data is collected from the back panel of controller. When the zero key on the controller front panel is pressed, it resets the present displayed value to “0.0000.” By considering this zero position as a reference, the increase and decrease are displayed as positive and negative numbers respectively. This function is used as a reference zero-point positioning. The LED indicates the measuring range by changing colors. The measuring range is 25 to 35 mm and the stability LED indicator lights yellow within this range. When the target is at the center of measuring range, approximately 30 mm away from sensor head the stability LED indicator lights green. The controller is wired to the National Instruments NI USB – 6008 data acquisition system to collect the analog output from the sensor and this data acquisition is graphically programmed in LABVIEW to store the data into excel files.

3.1.4 Laser Doppler Vibrometer

The laser vibrometer is a scientific instrument used to make non-contact vibration measurements of a surface. We use a Polytec Scanning Vibrometer PSV – 300 – F model. This consists of Controller OFV – 3001S, Scanning Head OFV – 056, Junction Box PSV – Z – 040 – F, Workstation and a heavy-duty tripod with motorized pan-tilt stage PSV-Z-017. The vibrometer is shown in 3.7.

Figure 3. 7: Laser Vibrometer

The decoders and filters in the controller as well as the data acquisition board in the workstation determine the characteristics of the PSV. Depending on the application there are three different models: High performance, High Frequency, and Universal. The 'F' in over model represents High Frequency. The junction box is connected to the controller interferometer, the controller RS-232 is plugged into the workstation. Computer monitor,

keyboard and mouse are connected to the workstation. The junction box has various setting such as external trigger, acoustic gate unit, signal output function generator, sync pulse, reference signal and input. The input of junction box is connected to the output of the controller. The scanning head is connected to the junction box and is placed on a pan-tilt stage. A Close-Up Unit OFV – 056 – CF99 is fixed on the front of the scanning head which is suitable for scanning very small parts.

3.2 VALIDATION OF EXPERIMENTAL APPARATUS

The experimental apparatus was validated to estimate static and dynamic characteristics of treated ligaments. Validation is necessary to show the repeatability of measurements and establish accurateness of the apparatus. These validation tests are discussed further.

3.2.1 STATIC CHARACTERISTICS

The goal of static testing is to analyze stiffness, maximum load to failure and energy consumed to break ligament from load-displacement graphs. Data obtained from "custom-built" load frame, load and displacement, were recorded using a LabVIEW program to generate load-displacement graphs.

A virtual instrument was programmed with all connections as in real-time and interfaced with hardware to access the equipment. The snapshot of the program written for these experiments is shown in Figure 3.8.

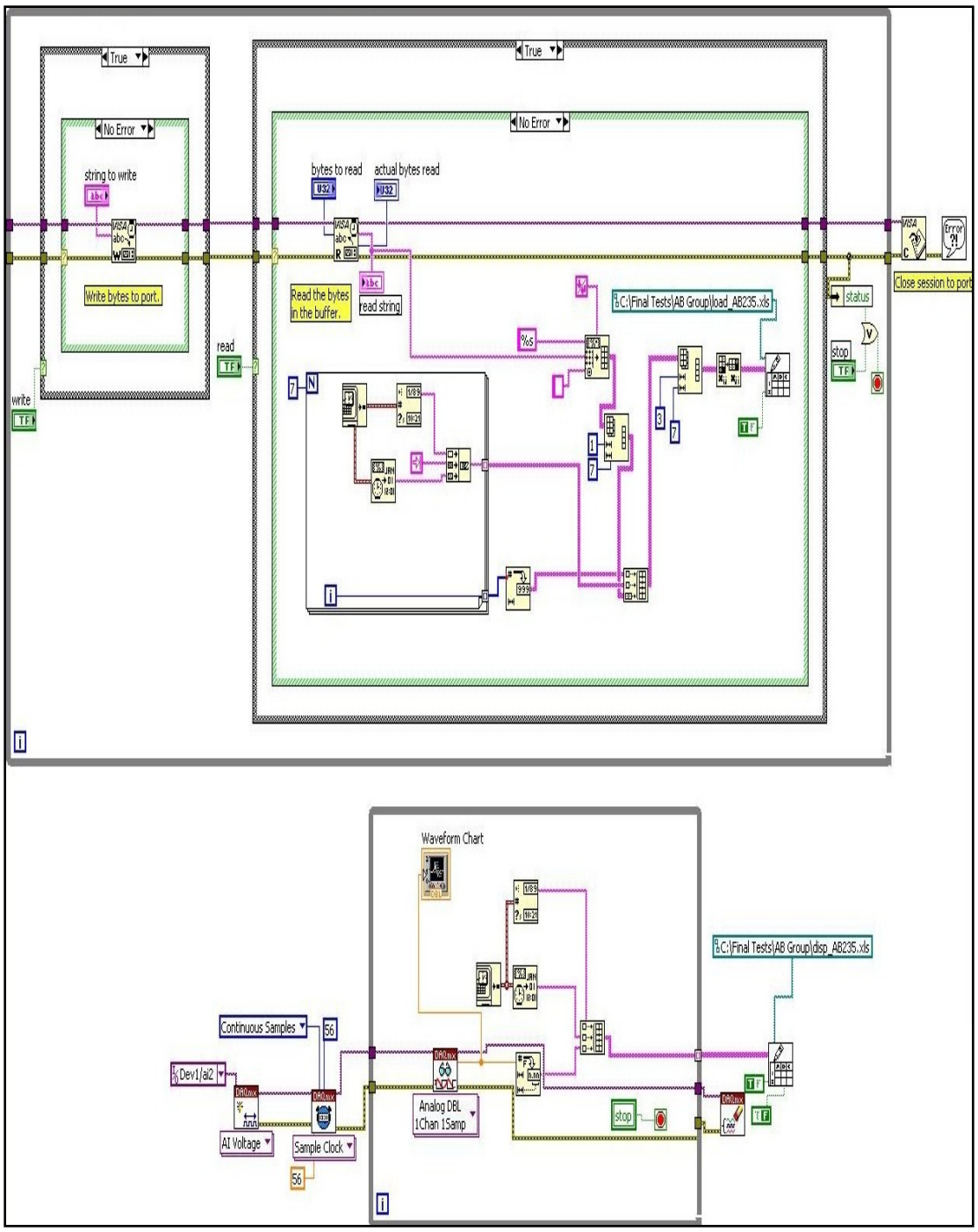

Figure 3. 8: Snap shot of LabVIEW program required to record data from load cell and laser sensor

To establish these characteristics “custom-built” load frame is validated in two methods. One, using a spring and then using sample non-treated ligaments.

Validation of "Custom-built" load frame using spring

Initially, the apparatus was operated using the picomotor and micrometer and results of each were compared and analyzed with the general lab test process using mass hanger, masses and vernier calipers. A spring along with mass hanger was hung using a hook. The mass hanger was loaded with various calibrated weights and the elongation of spring was measured with the laser sensor. Load vs. Displacement graphs were generated using this data. This experiment initially employed a high tension spring. The results of this calibration are shown in Figure 3.9. Note the large variation in the curves depending upon the technique used.

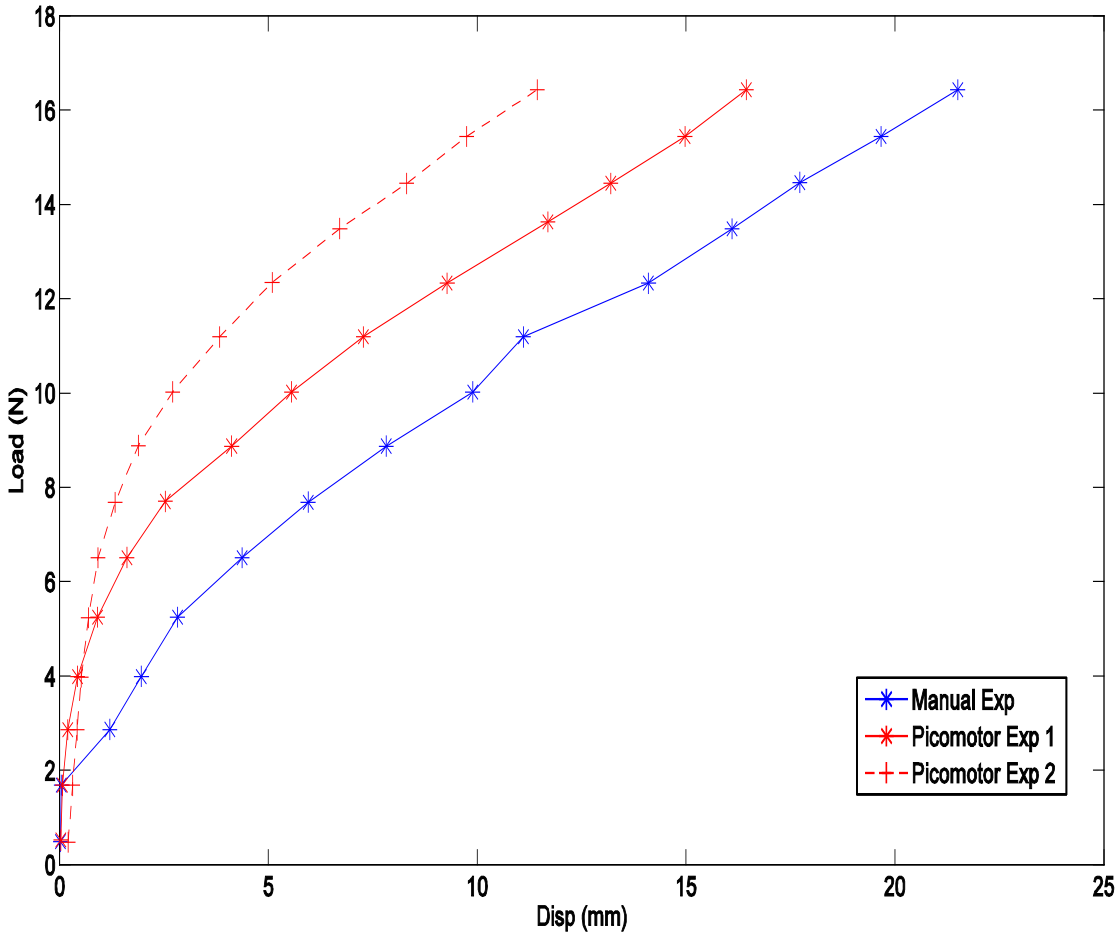

Figure 3. 9: Initial Load vs. Displacement graph of high tension spring showcasing variability

We reran the experiment using a spring with a lower spring constant whose safe working load is 5.28 lbs to check repeatability. Results are presented in Figure 3.10.

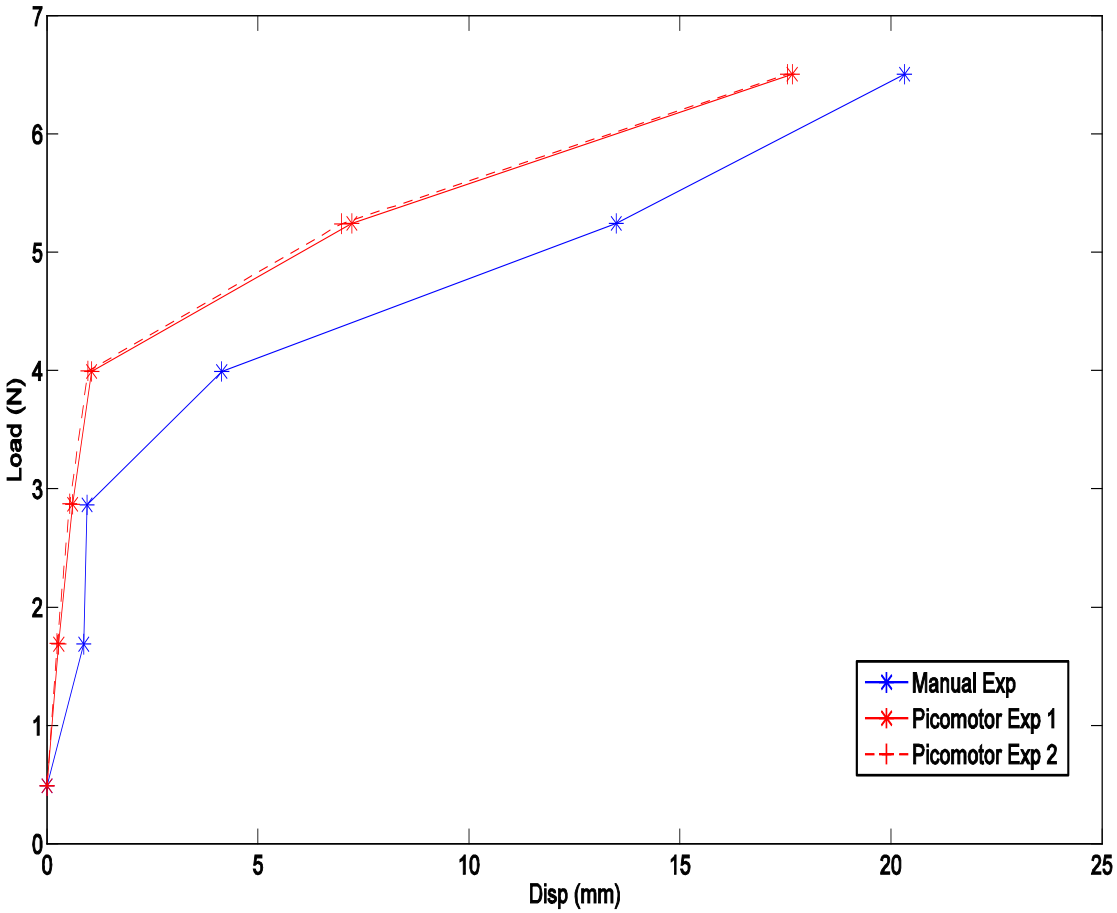

Figure 3. 10: Load vs. Displacement graph of spring of safe working load 5.28 lbs to detect accuracy of picomotor

In this case the picomotor readings were consistent but not in agreement with the manual test. To inspect the accuracy of the picomotor, picomotor was replaced by micrometer. The results in Figure 3.11 illustrate that although all tests were not consistent, the slopes are similar. Further improvements were made by increasing the sampling rate. Results are shown in Figure 3.12. However, the results still were not consistent.

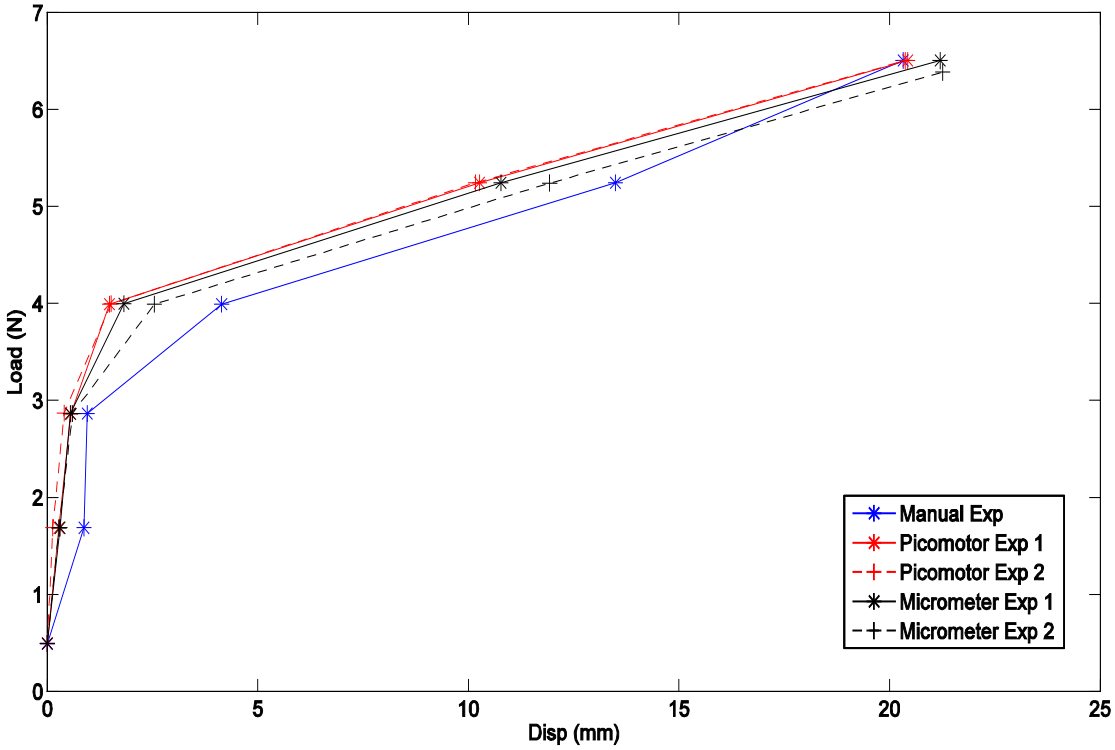

Figure 3. 11: Load vs. Displacement graph of spring of safe working load 5.28 lbs to validate picomotor and micrometer

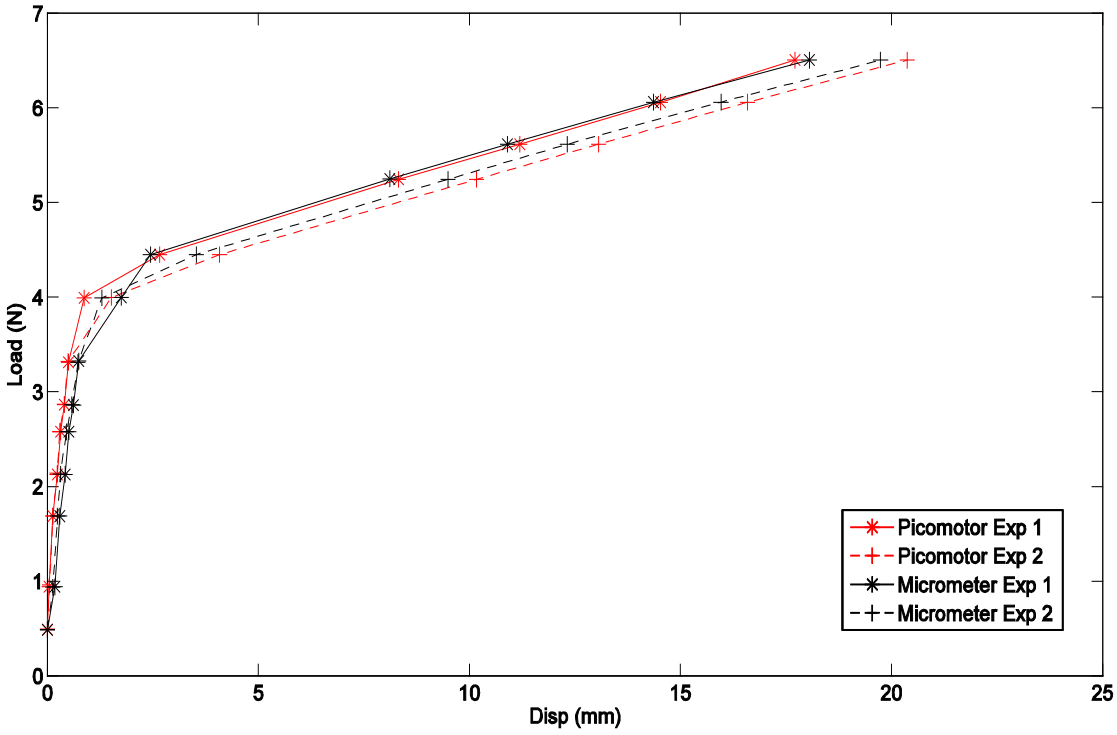

Figure 3. 12: Load vs. Displacement graph of spring of safe working load 5.28 lbs with high sampling rate to determine accuracy of picomotor and micrometer

As a next alternative, the tension of spring was further reduced. Now the safe working load of spring was achieved at 2.4 lbs. Figure 3.13 proves the tests are repeatable with reduction in tension.

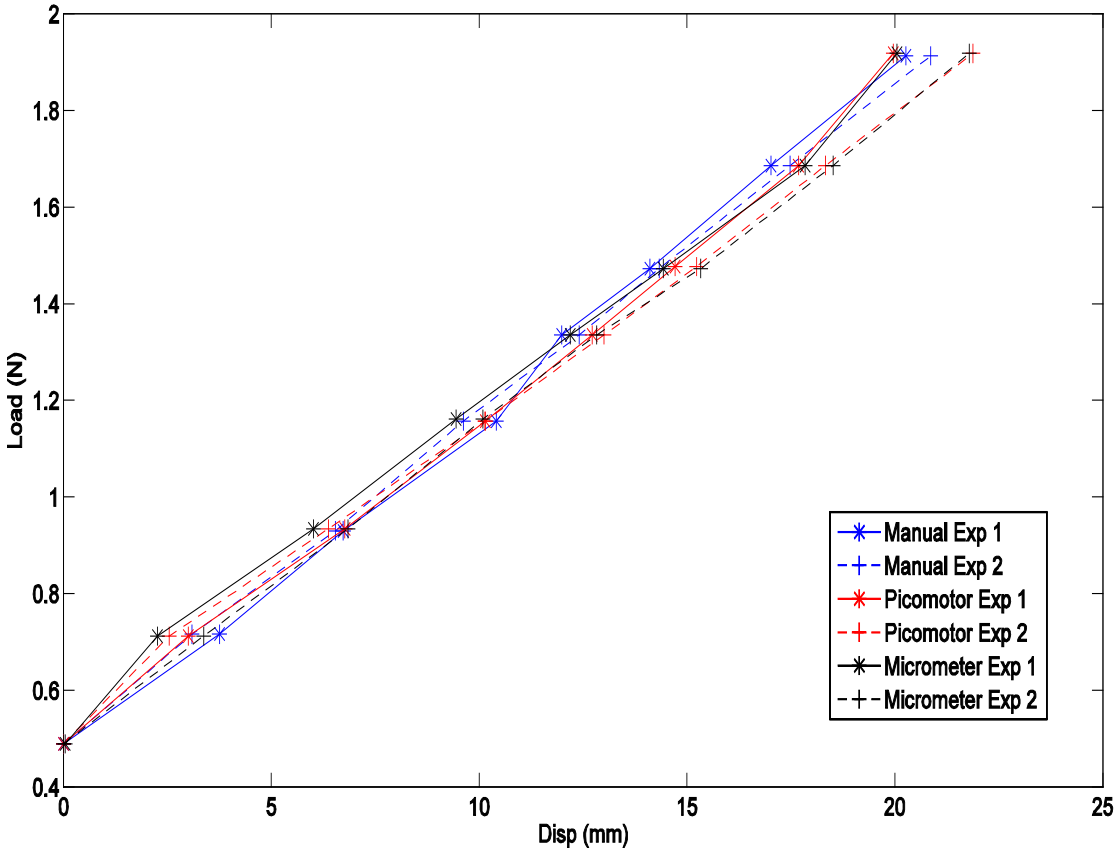

Figure 3. 13: Load vs. Displacement graph of spring of safe working load 2.4 lbs showcasing repeatability of data

Basic straight line fit graphs are generated for the data obtained from picomotor readings to examine slope of the lines. Standard deviation of slope and y-intercept of 3 picomotor tests are 0.0029 and 0.0201 respectively. Y-intercept conveys information regarding the start point. Difference of y-intercept establishes experiment initial point is different for the tests.

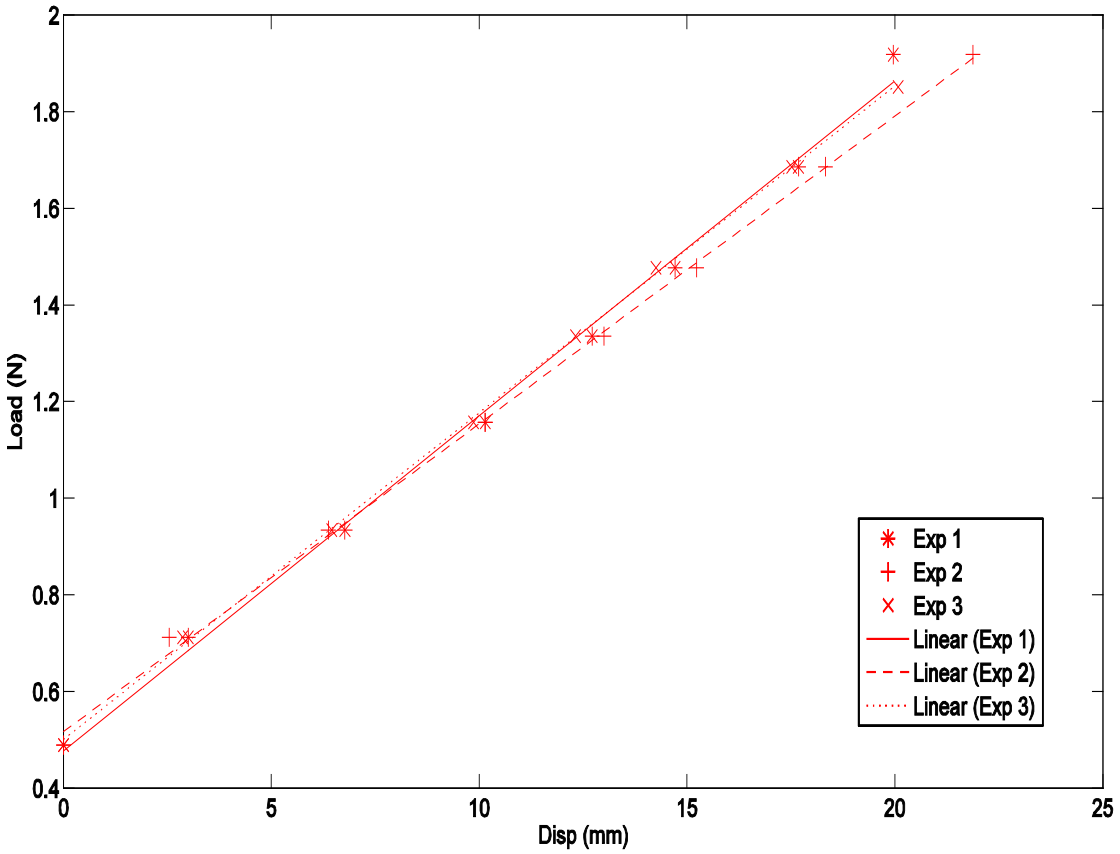

Figure 3. 14: Straight line fit of Load vs. Displacement graph of spring of safe working load 2.4 lbs to determine slope of curves

All tests performed by picomotor and micrometer are compared with manual test results. A manual test consists of mass hanger to which loads are added. Mass hanger adds a load of 0.4893 N. To balance all our tests we had a pre load of 0.4893 in picomotor and micrometer tests. A slight difference in a start point during repetitive tests might be a reason for a high standard deviation of y-intercept. To minimize this irregularity, a test with no load was performed using a picomotor.

Figure 3.15 shows that the picomotor duplicates results except when it is fully loaded. Basic straight line fit graph generated for these tests show standard deviation of slope and y-intercept to be 0.0005 and 0.0057 respectively. Results are displayed in the

consecutive Figure 3.16. This concludes results are repetitive when the start point is same and thus setup is successfully validated.

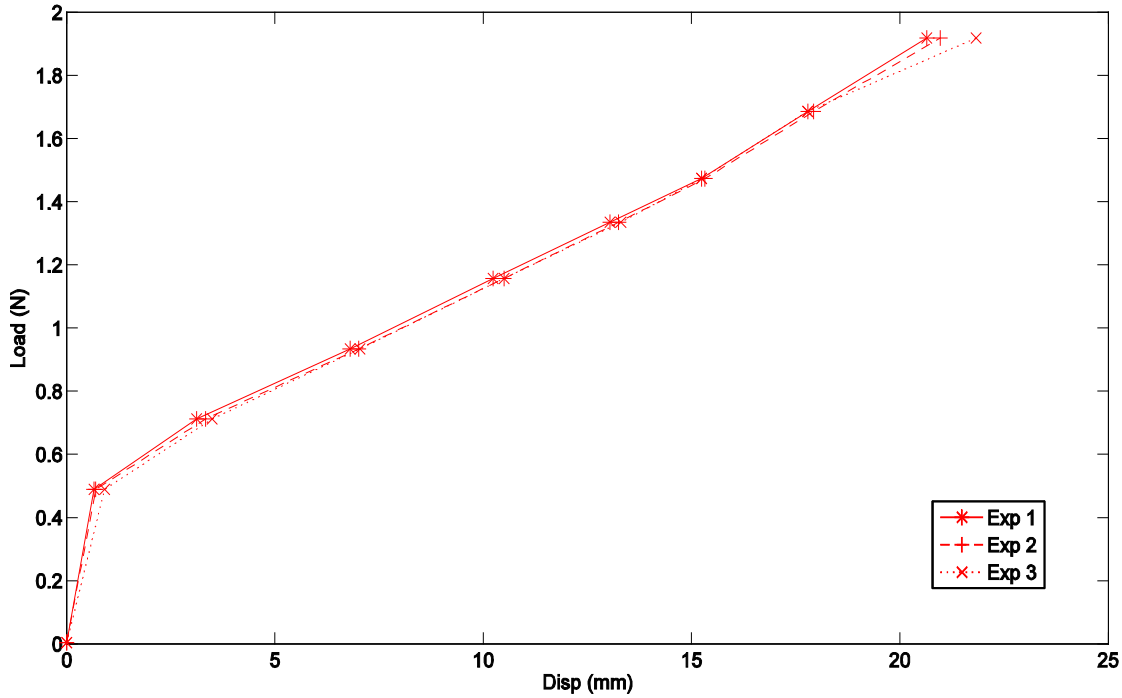

Figure 3. 15: Load vs. Displacement graph of spring of safe working load 2.4 lbs for picomotor

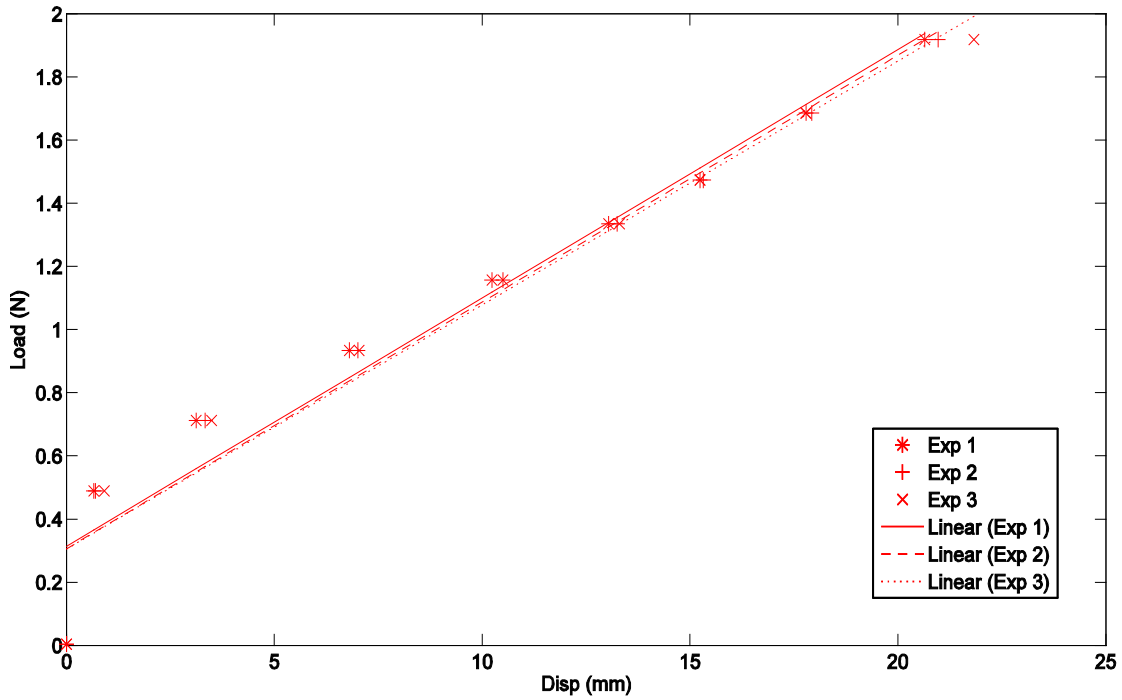

Figure 3. 16: Straight line fit of Load vs. Displacement graph of spring of safe working load 2.4 lbs for picomotor to determine slope and represent accuracy of results

Validation of "custom-built" load frame using non-treated ligaments

A set of preliminary experiments were performed on control (non-injured, non-treated) ligaments. Before mechanical testing the rat femur – MCL – tibia (FMT) unit is taken out of a -20°C refrigerator for thawing in a 4°C refrigerator for approximately an hour. Later, they are taken out of the refrigerator and cleaned free of fibrous tissue, skeletal muscle and other fascia surrounding the knee capsule. During this cleaning process the FMT specimens came to room temperature.

The FMT unit was then mounted on to the custom-built load frame using clamps, as shown in Figure 3.17. The clamps had sandpaper on their surface to hold the ligament tight without putting much pressure on the femur and tibia and prevent the bones from fracturing. After mounting, three ligaments (Anterior Cruciate Ligament (ACL), Lateral Collateral Ligament (LCL) and Posterior Cruciate Ligament (PCL)) were surgically transected to allow only the MCL and menisci to remain in contact with the bones. The MCL was kept moist by wetting it continuously by the application of a Phosphate Buffered Saline (PBS) solution to the exposed tissue.

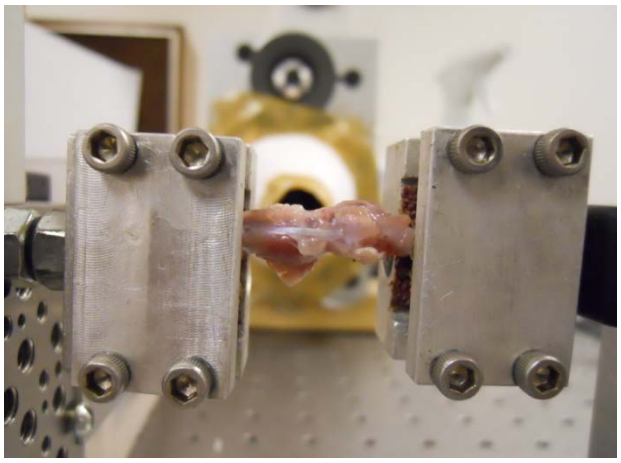

Figure 3. 17: MCL unit mounted on clamps

For each ligament, a static test was performed three times to show evidence of repeatability. Figure 3.18 and 3.19 show that the results were not only inconsistent but there was also some compression induced in the ligament or pre-load on the ligament. Due to this compression or pre-load the results were not consistent.

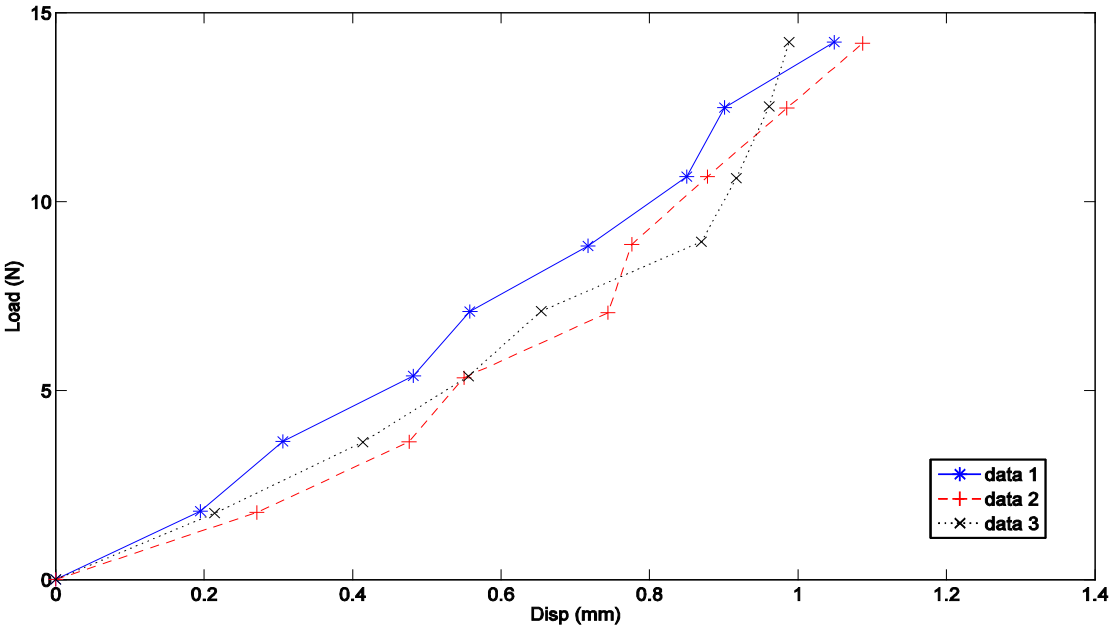

Figure 3. 18: Load vs. displacement of the initial test on ligament to check repetability

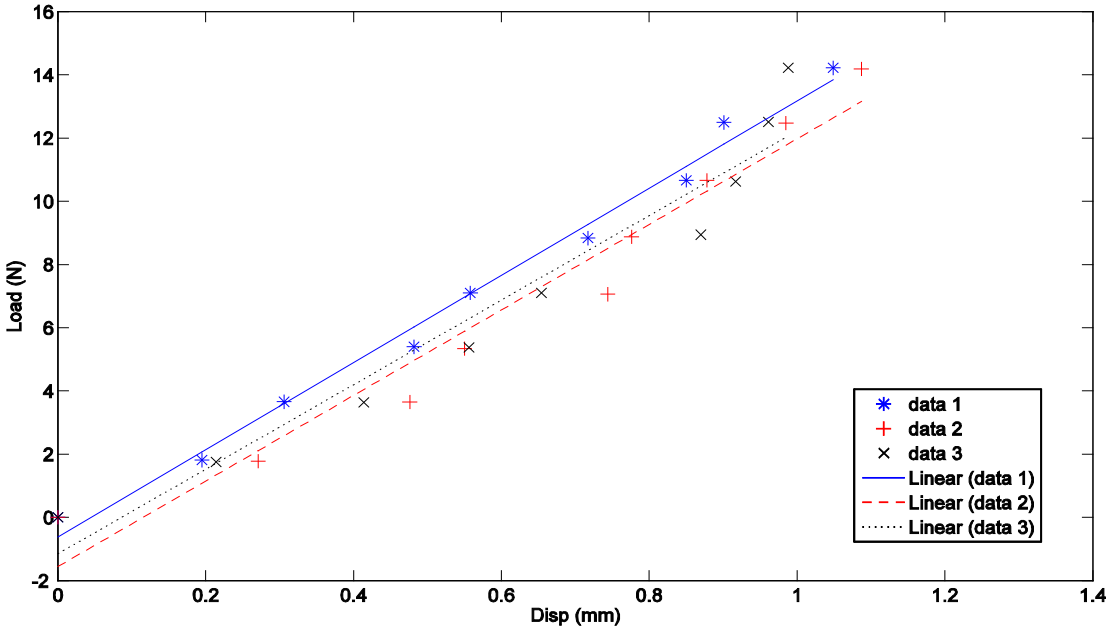

Figure 3. 19: Straight line fit of initial test on ligament to determine slope and confirm accuracy

One cause for compression may be due to varying shape of the articulating ends of the bones. The medial collateral ligament is attached to the femur and tibia. The femur is larger in diameter than the tibia. When the femur is mounted within the aligned clamps, one of the long bones undergoes compression and this compression is translated into the ligament. In order to minimize the compression phenomena, the clamps were moved fore and aft according to placement of the bones. Some reduction in compression can be viewed in the Figures 3.20 and 3.21.

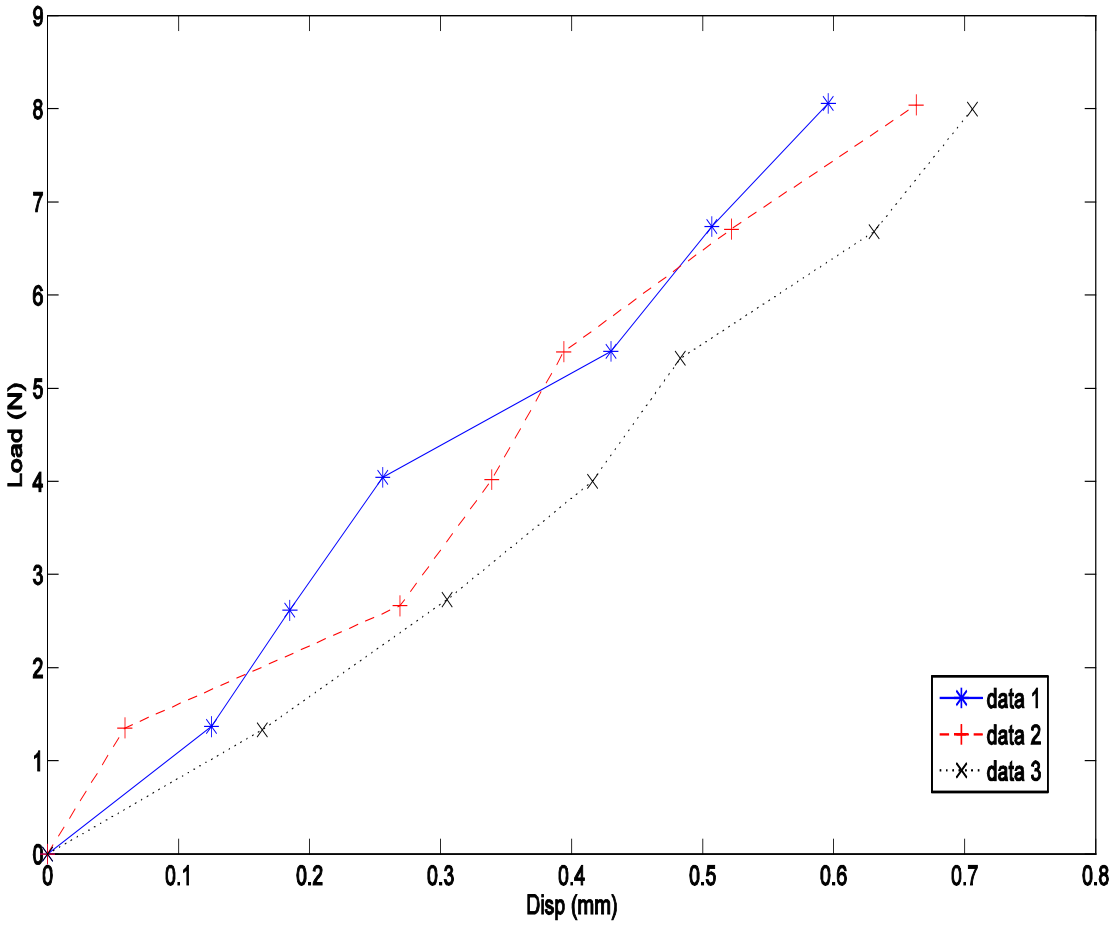

Figure 3. 20: Load vs. displacement for the test to minimize the compression on ligament

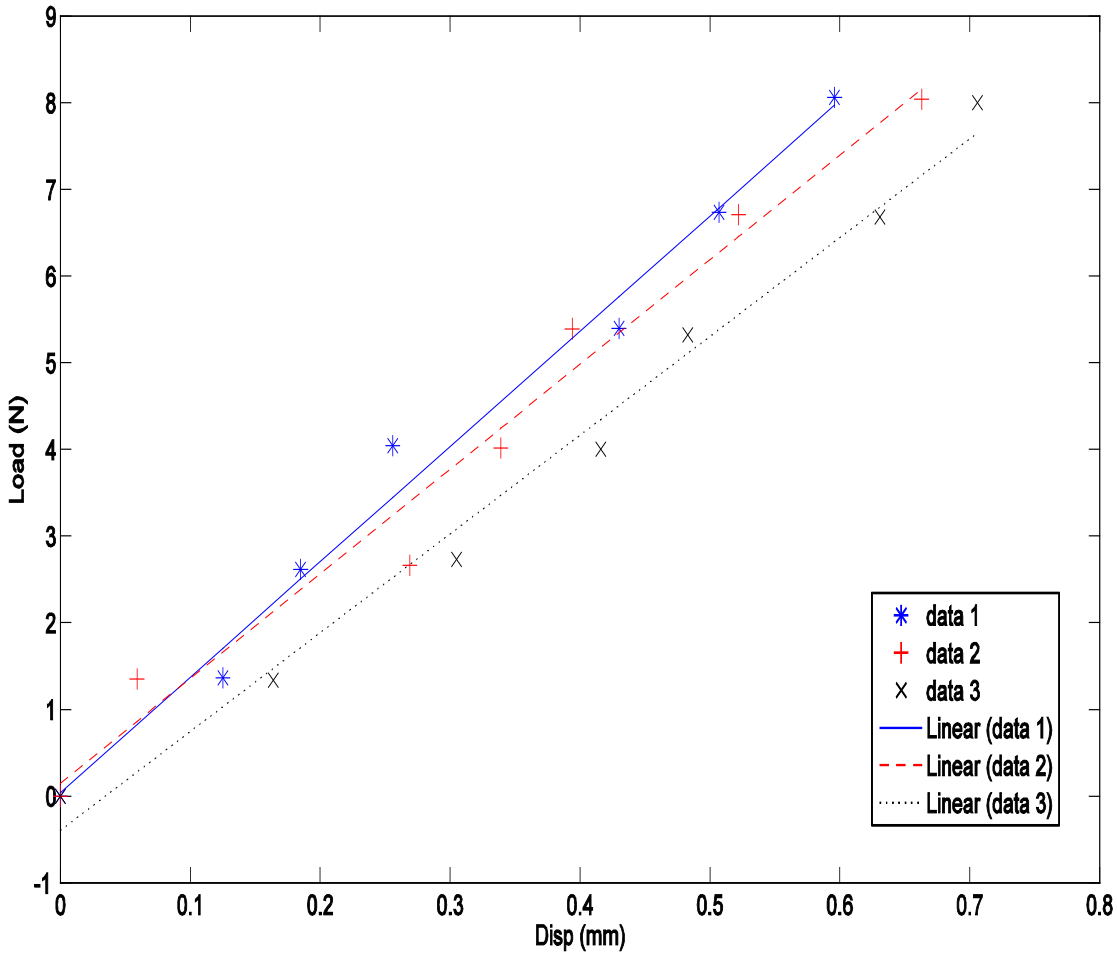

Figure 3. 21: Straight line fit of the test to minimize compression to determine slope and y-intercept

However, data inconsistencies were again reproduced. In order to alleviate the error variance included increasing the sample rate, an initial sample rate of 1 sample per second was subsequently change to 56 samples per second. When the sample rate was increased to 56 samples/sec, we determined the inconsistency was due to noise emanating from the laser sensor. The averaging of the fluctuating data also resulted in inconsistent data as seen in Figures 3.22 and 3.23.

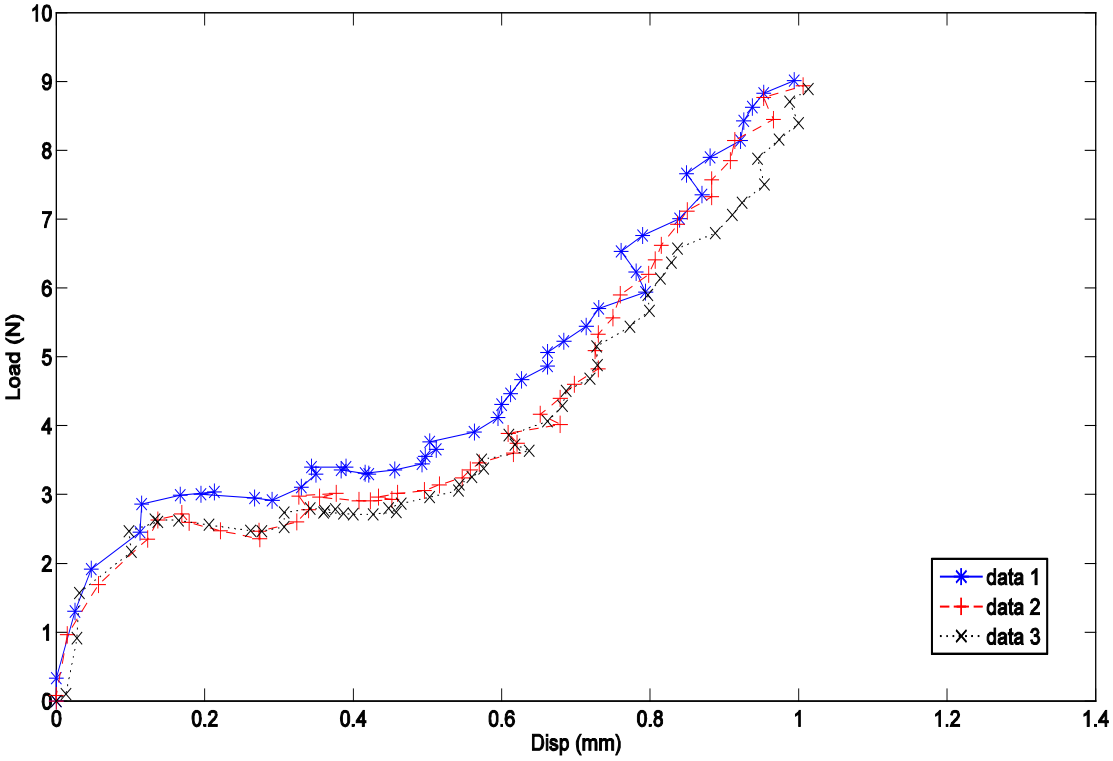

Figure 3. 22: load vs. displacement of averaged data of the test with high sampling rate to check repeatability

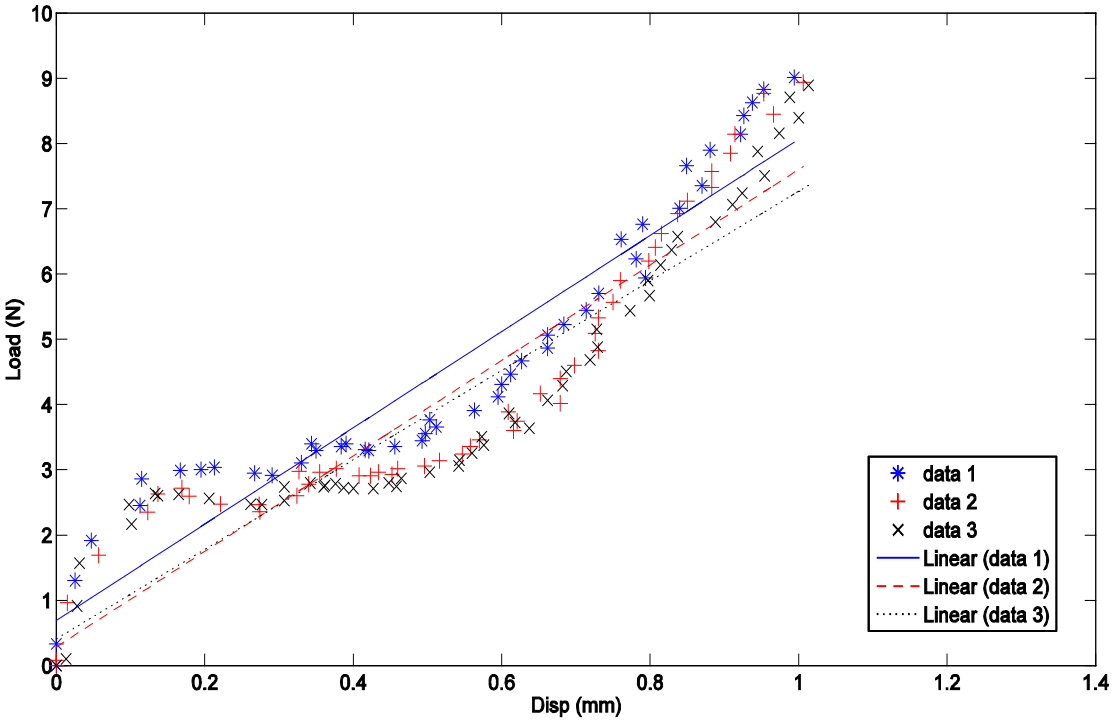

Figure 3. 23: Straight line fit of averaged data of the test with high sampling rate to estimate slope of curves

The replacement of the faulty laser sensor with a highly accurate nano-laser sensor was considered another possible solution. Our original laser sensor measuring range (±40 mm) and resolution (10 µm) lacked sensitivity. To minimize this precision problem the laser sensor was replaced with a nano-laser sensor with a measuring range of ±5mm and a resolution of 0.01 µm, which is more in accordance with the small animal specimens we routinely test (e.g., 0.001 mm). Figure 3.24 shows the raw data acquired from the nano-laser sensor with a sampling rate of 56 samples per second.

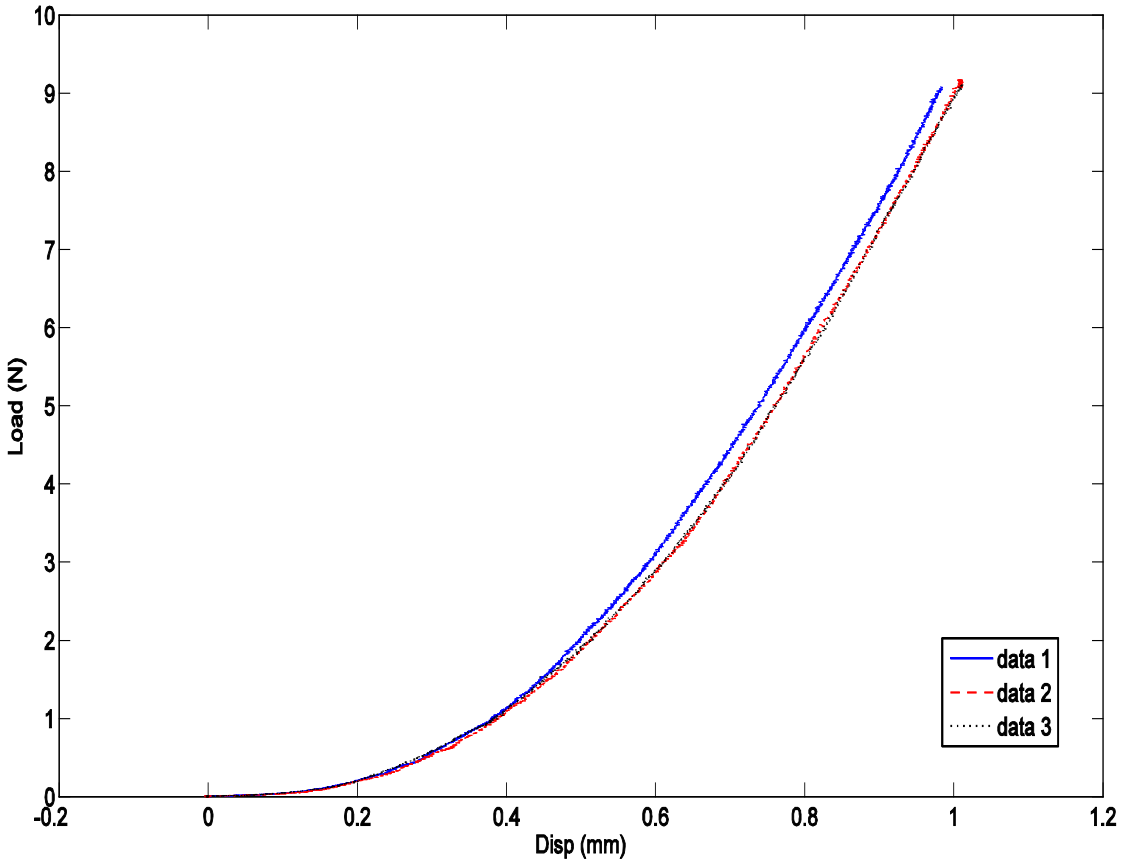

Figure 3. 24: load vs. displacement of test with high sampling rate and nano laser sensor displaying the accuracy in measurements

Figure 3.25 depicts the averaged data of the nano-laser sensor after multiple data acquisitions. We feel confident that our measuring apparatus possesses the needed accuracy and reproducibility required to produce reliable results.

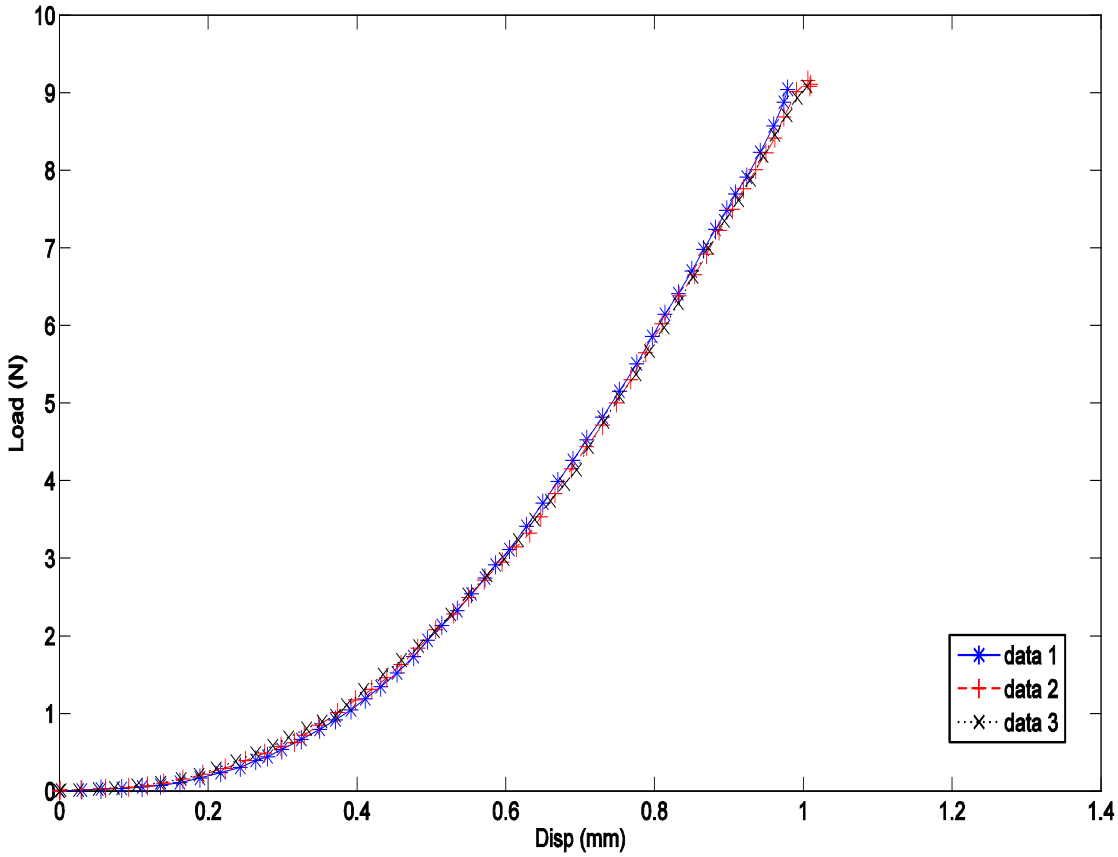

Figure 3. 25: load vs. displacement of the data averaged w.r.to one sec of the test with high sampling rate and nano laser sensor

3.2.2 DYNAMIC CHARACTERISTICS

The goal of the dynamic testing was to analyze the stiffness of the ligament from the resonance frequency of the tissue and determine the mode shapes at that frequency. We hypothesize that for a given healing ligament and treatment modality, there will be a differential stiffness that is proportional to a change in resonance frequency. The resonance frequency of a healing tissue will provide key information about the dense fibrous connective tissue without having to destroy the tissue in typical static biomechanical measures.

The laser vibrometer was validated to perform vibration measurements and the software PSV 7.41, a product of Polytec, was used to operate the vibrometer. The

software generated a function generator to give out an excitation and resultant vibrations are read by the laser vibrometer scan head and converted into digital signals. This software has several variables such as window, excitation, band width, FFT lines, sampling rate, amplitude with different options that can be chosen based on our requirement of output. To extract valid frequency information, the digitalization of the analog signal must occur at a certain rate or else the signal may be distorted. Quantization, Sampling, Aliasing and leakage are important during digitalizing an analog signal. When the measured signal is not periodic in the sample interval, incorrect estimates of the amplitude and frequency occur. This error is known as leakage. This can be minimized by window. Most common windows are Rectangular, Hanning, Flattop, Force and Exponential. Based on the signal, respective window is used to study the characteristics of signal. Rectangular, Hanning and Flattop are utilized for Shaker Excitation testing, Force and Exponential are used for impulsive excitation testing such as Impact testing.

Most commonly used impact device is a hammer. Most commonly used shakers for modal testing are electromagnetic and electro hydraulic types. The force inputs given to the shaker are generally classified into two categories. They are Deterministic and Random Signals. Each of these signals is used to determine the characteristics of the system such as generation of frequency response function and linearity of system. Some examples of deterministic signals are sine chirp, swept sine and digital stepped sine. Some examples of random signals are pure random, burst random, pseudo random and periodic random.

In our set of experiments we used periodic chirp excitation with a rectangle window. Frequency Band Width is 500 Hz. Recorded data is used to generate Frequency response functions (FRF) and operating deflection shapes (ODS). ODS gives the dynamic behavior of the structure (He and Fu 2001; Schwarz and Richardson 1999). FRF are generally used to describe the input-output relationship of the system. Different algorithms such as H_1, H_2, and H_v are used to estimate FRF's. Algorithms are selected based on the requirement. Most frequent formulation FRF uses H_1 algorithm as it minimizes the noise on the output (Broesch, Stranneby, and Walker 2008; He and Fu 2001; Ewins 2001). We used H_1 FRF's to determine the resonant frequencies in ligaments.

Validation of Laser Vibrometer using ligament

In pilot experiments, the ligament was positioned horizontally and a speaker was placed below the specimen to excite the ligament with sound. The vibrometer along with the "close-up unit" was mounted on the vertical stand and adjusted so that it now resides above the ligament. Positioning the speaker below the ligament failed to excite the small knee ligament. Thus, we tried to implement an impact excitation using a calibrated impact hammer. The data collected from this test contained a greater amount of noise making it difficult to determine the resonance frequency. This is shown in Figure 3.26.

To troubleshoot this new setback, we postulated that the impact hammer failed to provide the proper impact excitation to the ligament. Our laboratory procured a new speaker and subsequent studies suggest that the energy frequency band is sufficient to perform our tissue resonance energy experiments. In Figure 3.27 we can see the amount of velocity present in the frequency band we intended to perform experiments.

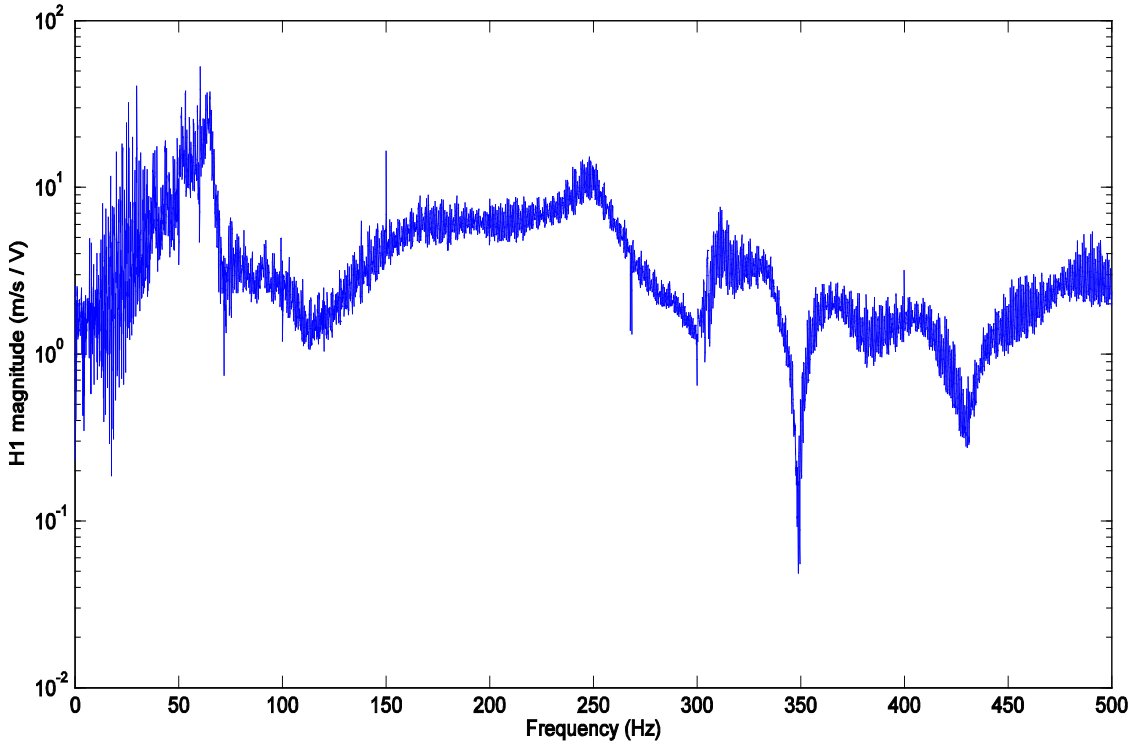

Figure 3. 26: Frequency Response Function (H1) of Impact Excitation showcasing no resonance due to presence of noise

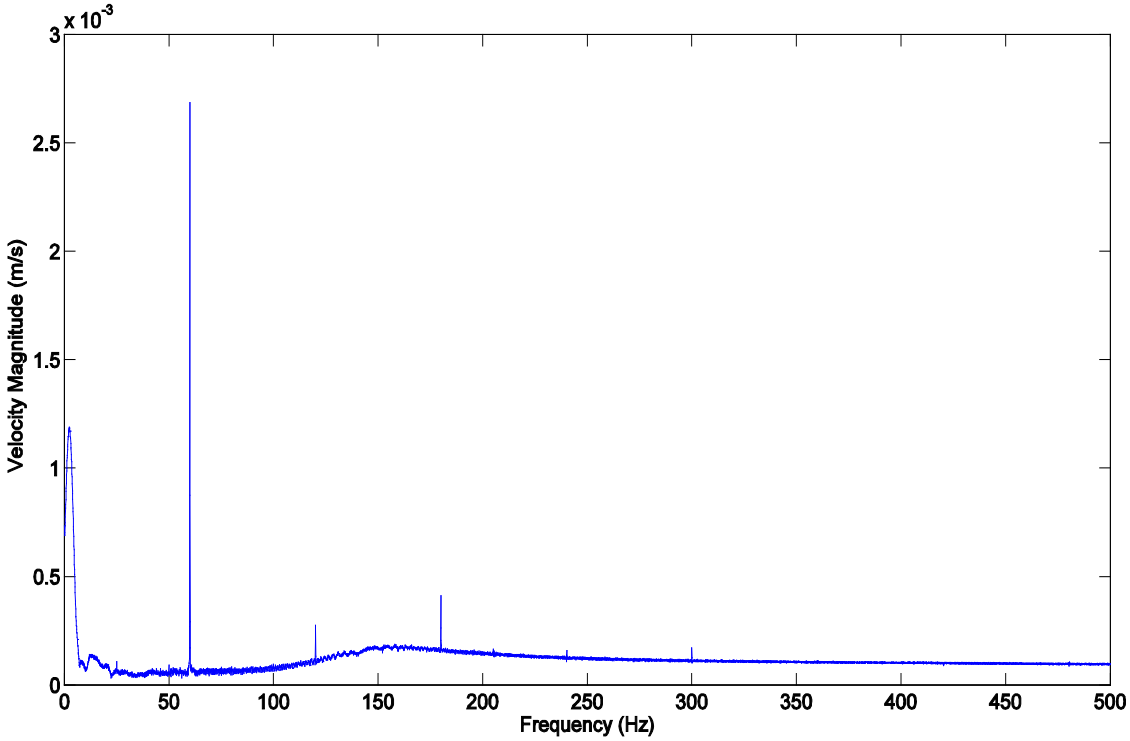

Figure 3. 27: Velocity Spectrum in Band Width 500 Hz displaying energy present in speaker

The results revealed that the clamp on the load cell side exhibits some motion due to the attachment of the clamp to the load cell and the load cell to the stand in a cantilever beam format. The speaker is placed behind the ligament while the vibrations are detected by the vibrometer placed in front of the ligament with the help of a pan-tilt stage. To focus the acoustic vibrations on ligament sound waves are directed to a point using a cone shaped attachment made of white paper to the speaker. The photographic view is shown in Figure 3.28. The data acquired still possesses motion in the clamps on the side of the load cell; however, we deem that this motion is negligible and should not impact our default conditions during our experiments.

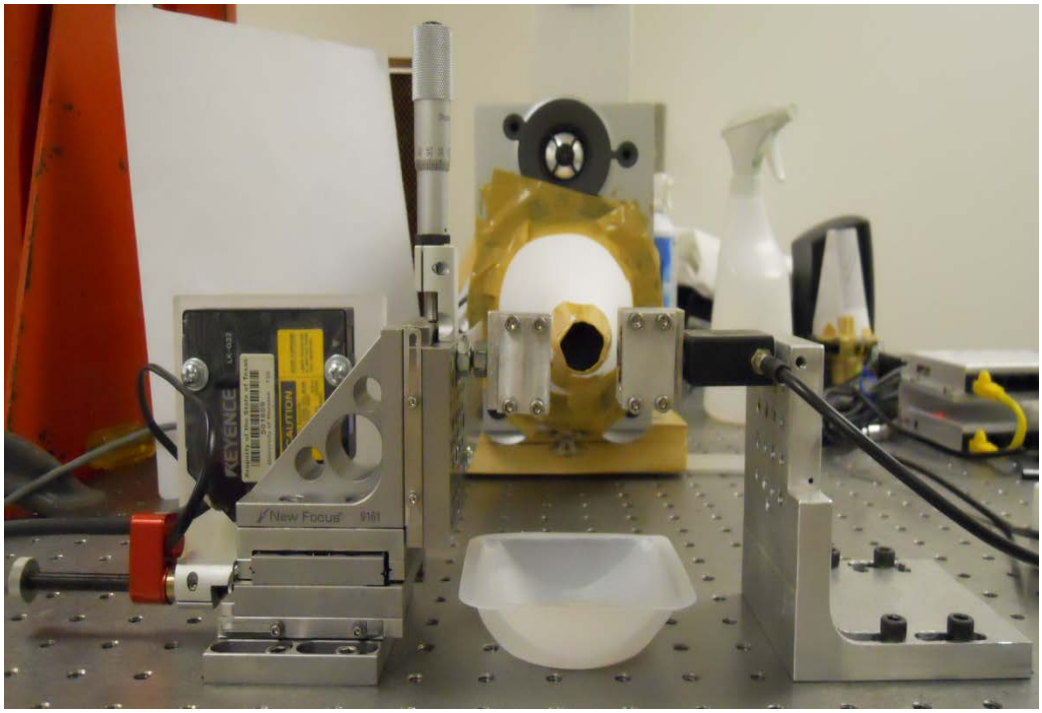

Figure 3. 28: Photographic view of Mechanical Apparatus showing position of speaker behind the clamps

Figure 3.29 displays a snap shot of laser vibrometer scanning video along the length of the ligament in varying shades of green pixels.

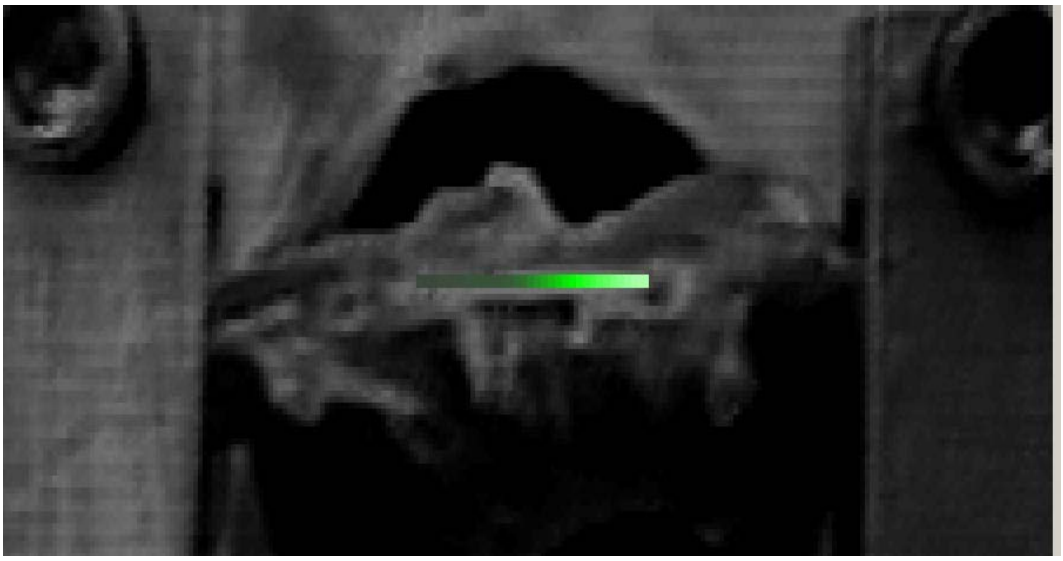

Figure 3. 29: Ligament displaying scan points for laser vibrometer scanning

The frequency response function H1 of the ligament is shown in the Figure 3.30. Resonance phenomena are noticed at 260 Hz and 435 Hz. Mode shapes corresponding to the resonance frequencies can be seen in the consecutive Figure 3.31. Thus, load vs. displacement graphs, frequency response functions, mode shapes of the control ligaments successfully validated the setup to perform further experiments on treated ligaments.

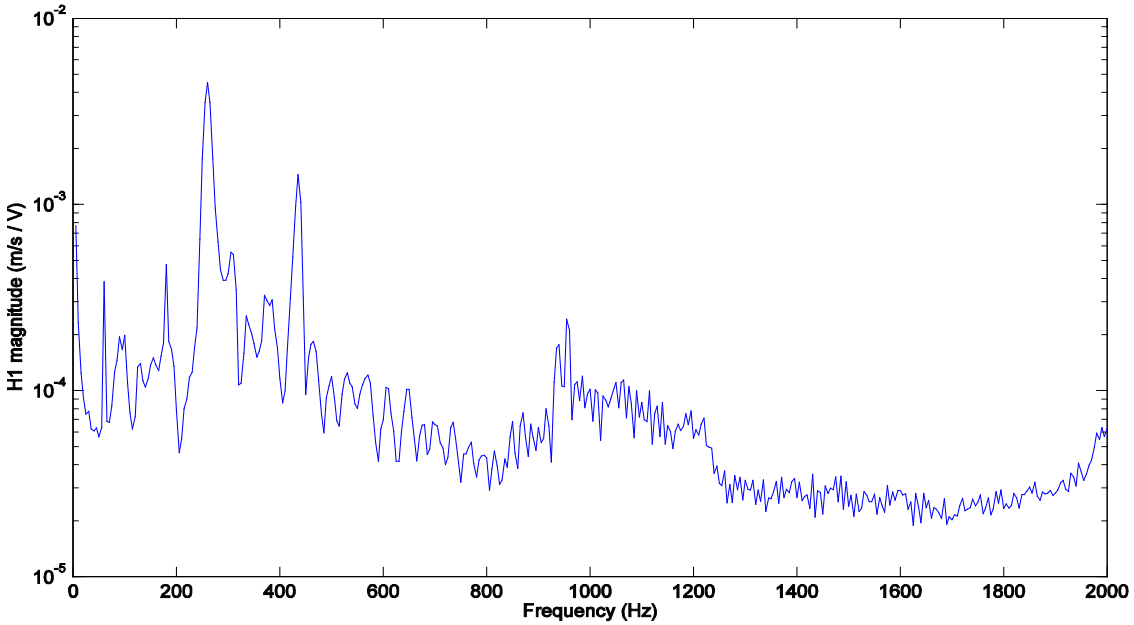

Figure 3. 30: Frequency Response Function (H1) of the ligament displaying Resonance frequency at 260 Hz and 435 Hz

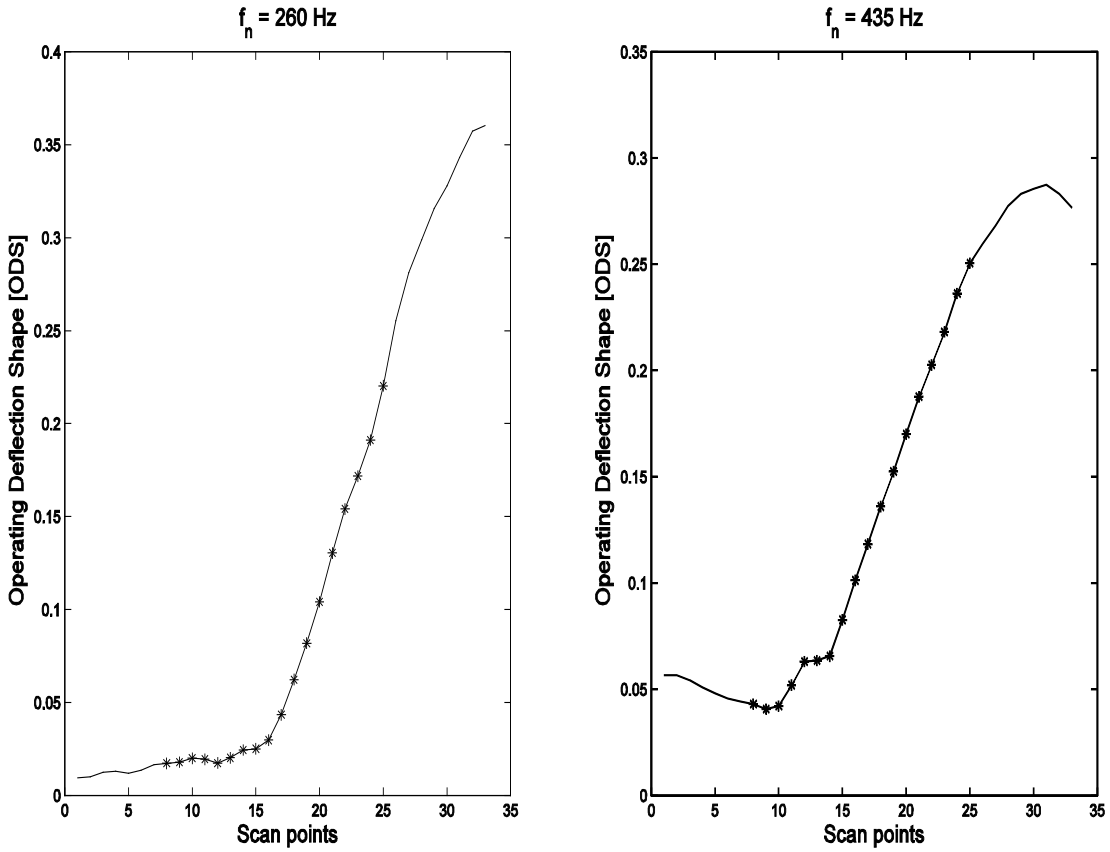

Figure 3. 31: Operating deflection shapes of the ligament at frequencies 260 Hz & 435 Hz representing the movement of the ligament under excitation

CHAPTER 4

RESULTS AND DISCUSSIONS

All treated ligaments were preconditioned at ~1% strain for 10 cycles. The FMT specimens were loading at a displacement rate of 1.2 mm/min until they reached 0.8 mm (~ 50% of strain) displacement. The picomotor movement was stopped and the speaker was turned on to apply the excitation while the resultant vibrations of the ligament were scanned by the laser vibrometer. This part of the testing took approximately 20-30 minutes. Once the ligament has been scanned for vibrations, the picomotor was commanded to increase strain at the same rate until the ligament failed.

Experimental results were divided into three parts. 1. Stiffness of the ligament after initial elongation. 2. Stiffness, Load to failure and Work to failure after 2^{nd} elongation. 3. Natural Frequencies, Frequency Response Functions and Operating Deflection Shapes measured during the relaxation period between 1^{st} and 2^{nd} elongation.

Statistical analysis was performed on recorded data. All data were expressed as means ± SEM and evaluated using the statistical package SAS (Rev 9.2.3; Cary, N.C.). To evaluate the differences among groups for each dependent variable, a one-way ANOVA was applied. When the F tests were significant, Duncan's post hoc tests and least square means were used to further identify differences between group pairs. Statistical significance level was set at $p < 0.05$. In the Figures, corresponding means with the same letters are not significantly different from each other ($p > 0.05$) [Obtained from D.A.Martinez].

4.1 RESULTS

4.1.1 Static Characteristics

Stiffness was calculated from the linear portion of the slope of the load-displacement graphs shown in Appendix A. Figure 4.1 displays a bar graph representation of the stiffness during the initial elongation. Significant differences were seen between Sham control ligaments from GFP, IGF-1a, IGF-1b, IGF-1a+1b treatment groups. Stiffness of sham group is significantly different from GFP, IGF-1a, IGF-1b, IGF-1a+1b groups ($p < 0.0001$). GFP, IGF-1a, IGF-1b, IGF-1a+1b were not significantly different from each other ($p > 0.05$).

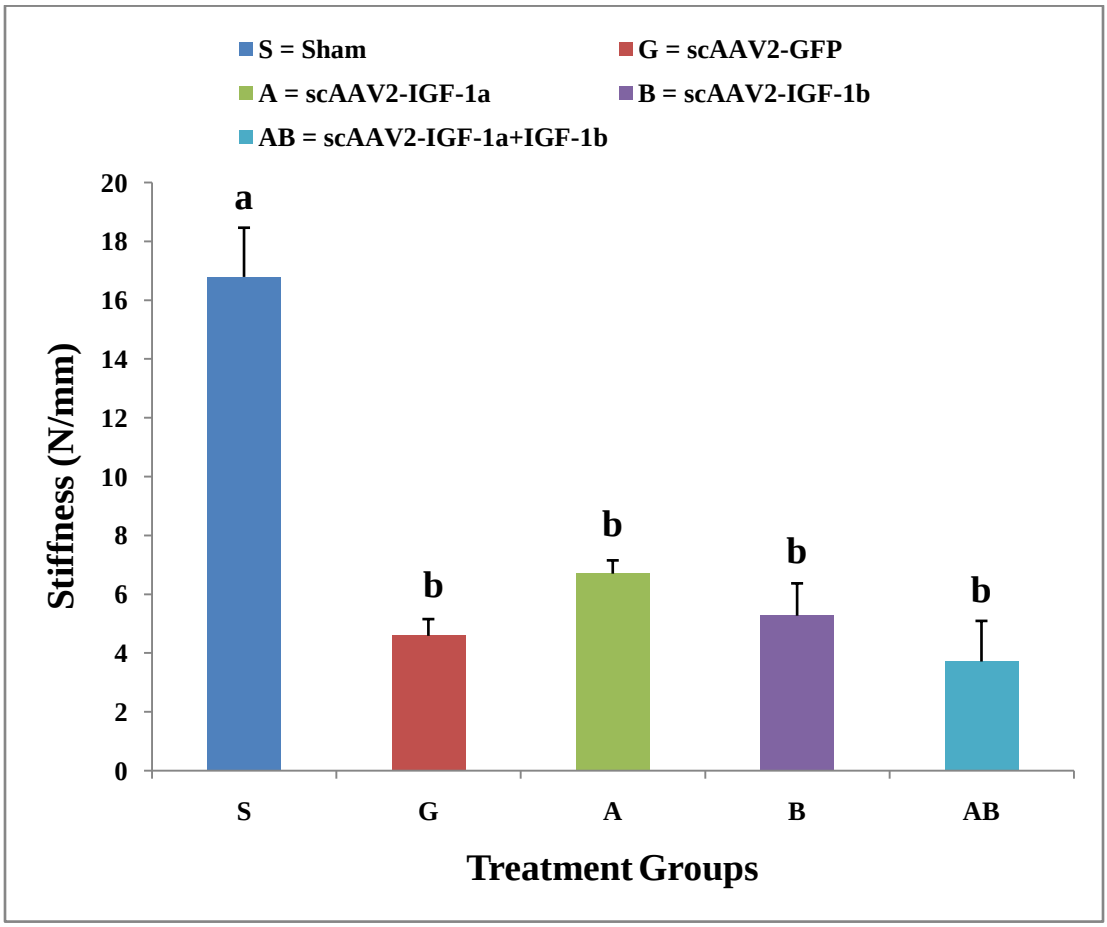

Figure 4. 1: Stiffness values (mean ± S.E.M)

The stiffness of each ligament after relaxation during the load to failure was determined in the same way using the second load-displacement curve. Related graphs are presented in Appendix C. Stiffness after relaxation noticeably increased in all treated ligaments compared to sham control group. Figure 4.2 shows significant stiffness increase in GFP, IGF-1a, IGF-1b treatments compared to IGF-1a+1b treatment. Stiffness of sham group is significantly different from GFP, IGF-1a, IGF-1b, IGF-1a-1b groups ($p = 0.0085$, $p = 0.0077$, $p = 0.0449$ and $p < 0.0001$ respectively). GFP, IGF-1a, IGF-1b stiffness significantly different when compared to IGF-1a+1b ($p = 0.0059$, $p = 0.0264$ and $p = 0.0019$ respectively).

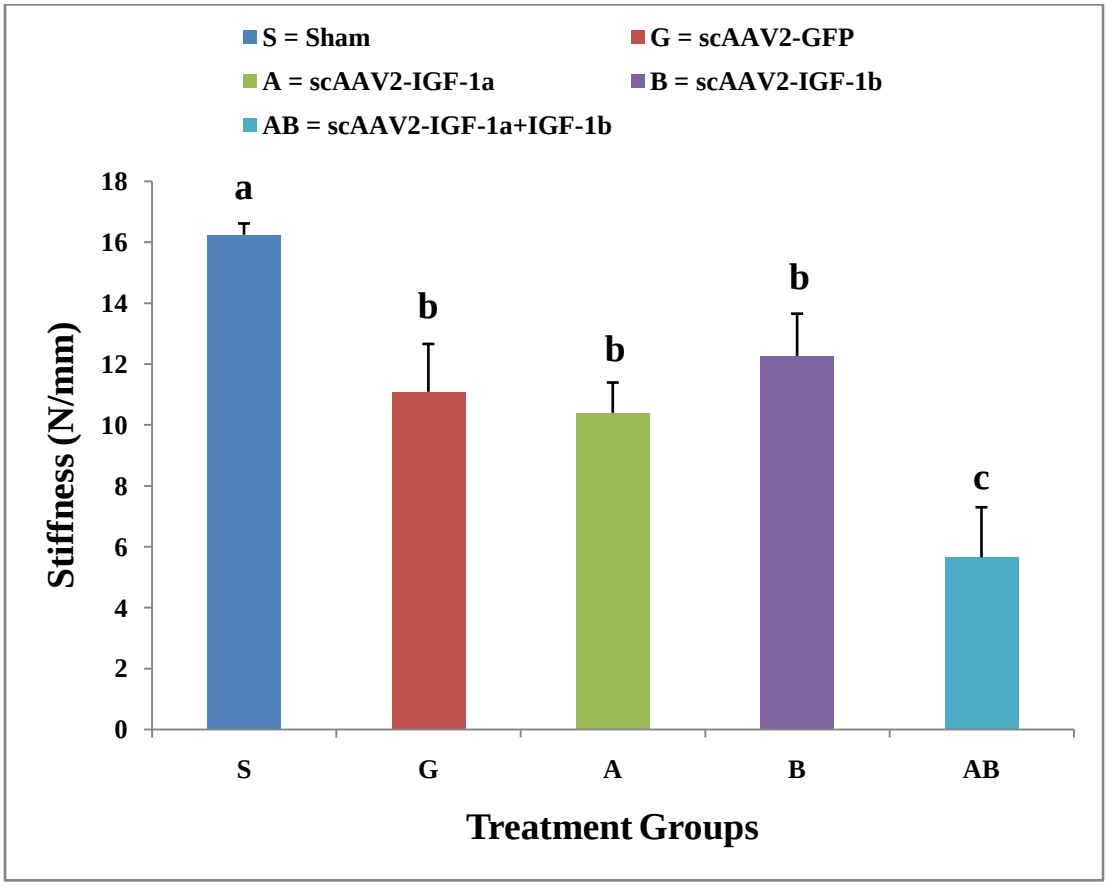

Figure 4. 2: Stiffness values (mean ± S.E.M)

Maximum load to failure values are extracted from the load-displacement graphs added in Appendix B. Figure 4.3 represents a graphical representation of the results. IGF-1b group significantly increased when compared to GFP, IGF-1a-1b groups ($p = 0.0482$ and $p = 0.0084$ respectively). There was a trend of the IGF-1b group to have a greater load to failure compared to the IGF-1a treated group ($p = 0.0675$), though not significant ($p > 0.05$).

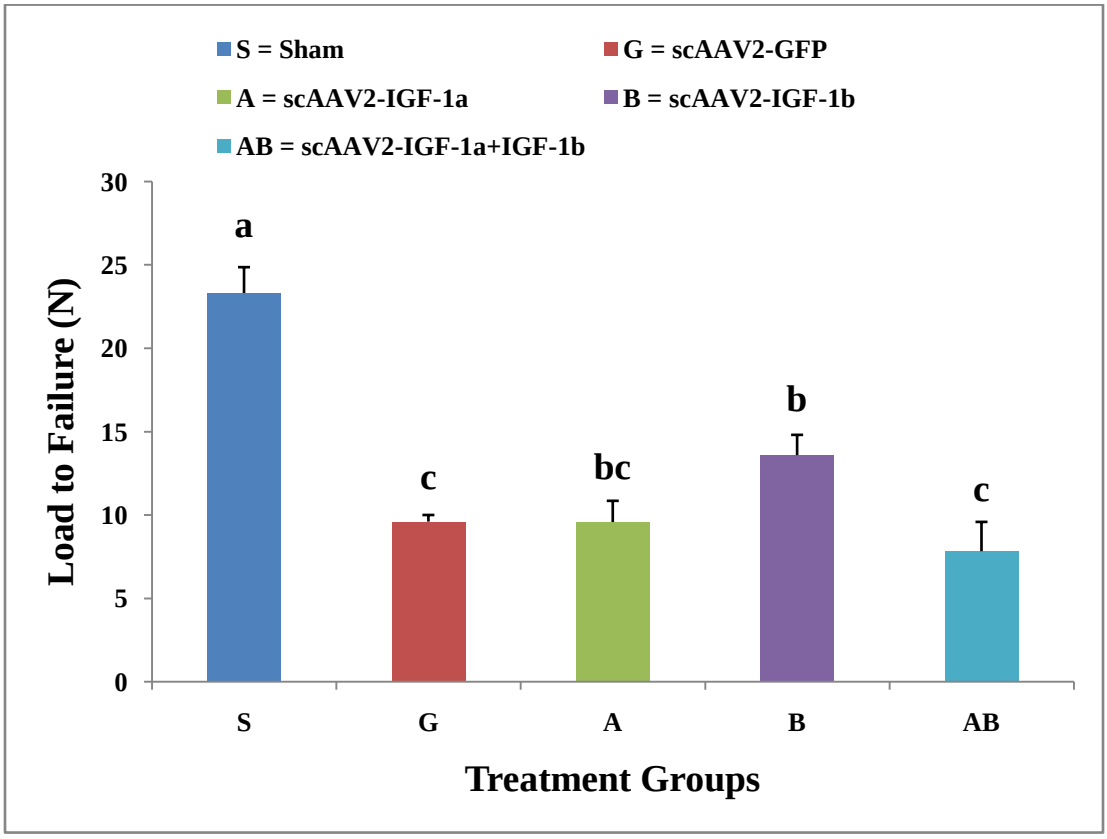

Figure 4. 3: Load to failure values (mean ± S.E.M)

Elastic storage energy was computed from load-displacement graphs referred in Appendix C. Figure 4.4 presents a bar representation of the results. IGF-1b is not significantly different from Sham group. This illustrates, ligaments treated with IGF-1b are as strong as the Sham group. IGF-1b group significantly increased when compared to GFP, IGF-1a, IGF-1a-1b groups ($p = 0.0118$, $p = 0.0007$ and $p = 0.0275$ respectively).

The Sham group and IGF-1b treated group are not significantly different from each other (p = 0.3382).

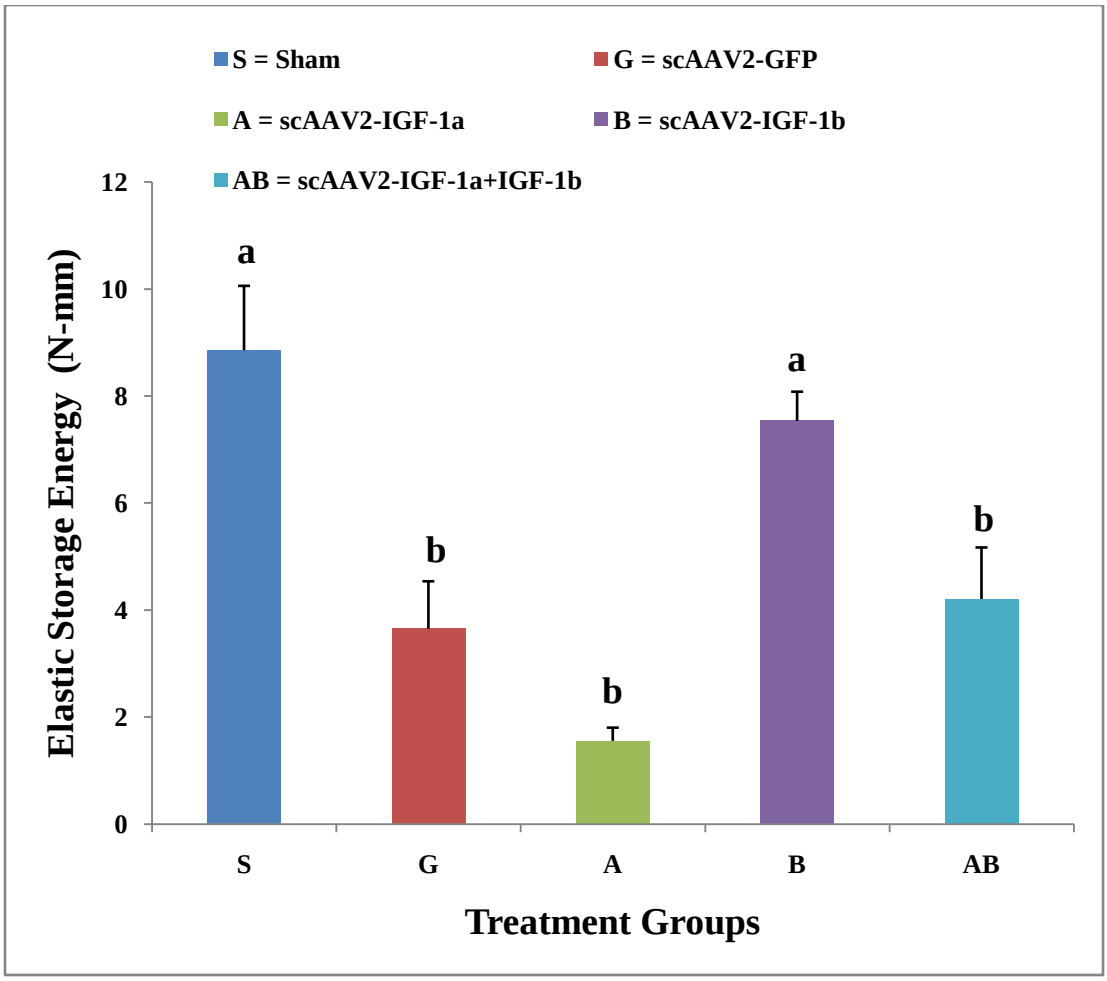

Figure 4. 4: Elastic Storage Energy values (mean ± S.E.M)

Work to failure was calculated from load-displacement graphs displayed in Appendix B. A graphical representation of results is shown in Figure 4.5. It demonstrates an increased significant difference of energy needed to disrupt ligaments in the IGF-1b treated group compared to GFP, IGF-1a, IGF-1a+1b treated groups. Also, IGF-1b is not significantly different from the Sham group. This suggests that ligaments treated with IGF-1b were as tough as ligaments from the Sham group. The IGF-1b group toughness

was significantly increased when compared to GFP, IGF-1a, IGF-1a-1b group toughness ($p = 0.0086$, $p = 0.0007$ and $p = 0.0292$ respectively). The Sham group and IGF-1b group toughness measures are not significantly different ($p = 0.4094$).

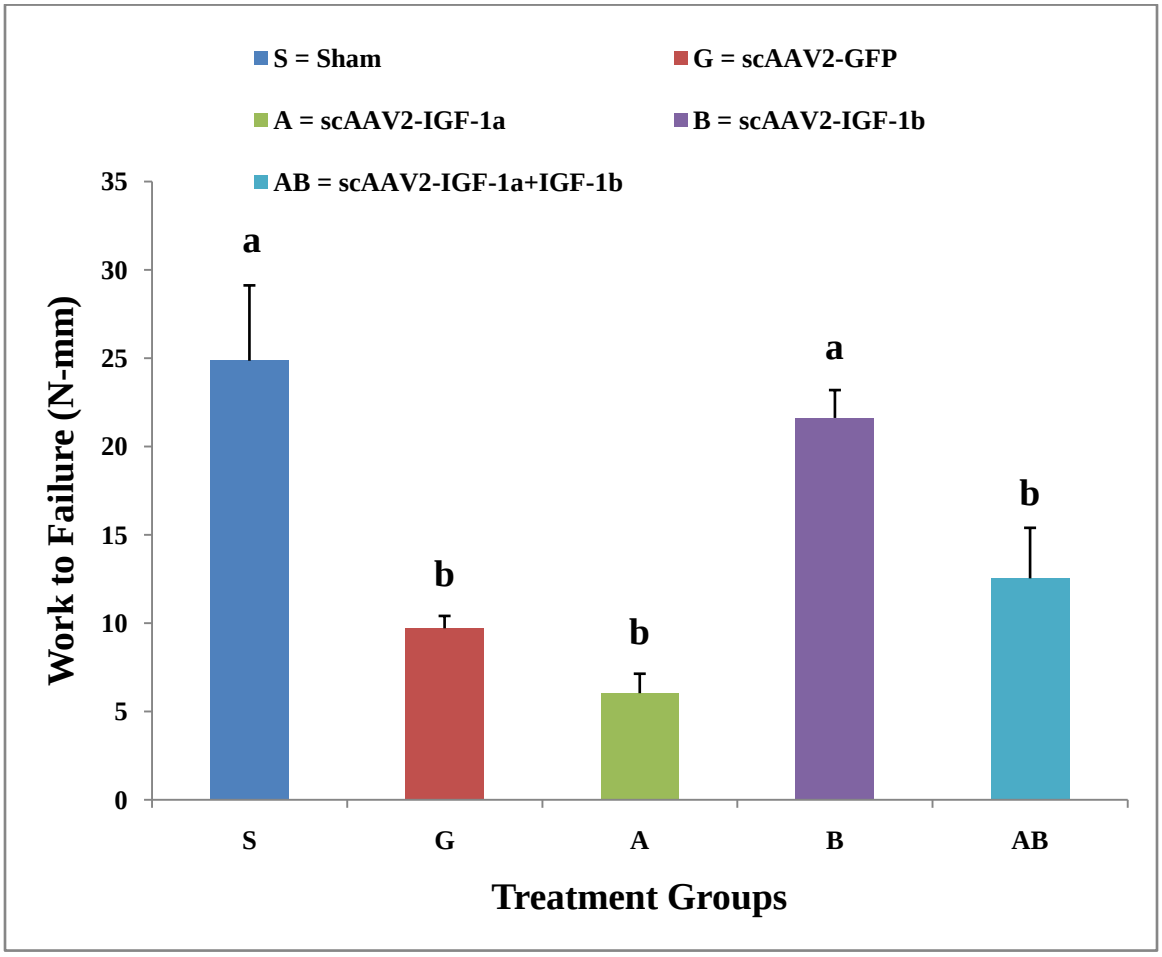

Figure 4. 5: Work to failure values (mean ± S.E.M)

4.1.2 Dynamic Characteristics

Frequency Response Function (FRF) was generated using parameters of excitation given by function generator in laser vibrometer and response-vibrations detected by laser vibrometer. Resonance phenomena can be noticed in the FRF's presented in Figure 4.6. Natural frequency related to 1st mode shape was very evident in graphs and 2nd mode is in process of formation. Numerical values of natural frequency of

each group are mentioned in the title bar of graph and then they are graphically represented in form of bar graphs in consecutive Figure 4.7. The natural frequency denoted here is (Mean ± SEM). Ligament frequencies are presented in Appendix D. Natural frequencies of treatment groups are significantly indifferent ($p > 0.05$). Operating Deflection Shapes (ODS) related to these natural frequencies (Mean ± SEM) are shown in Figure 4.8 in sequence. The highlighted points in the ODS denotes the area of ligament exposed to speaker from behind.

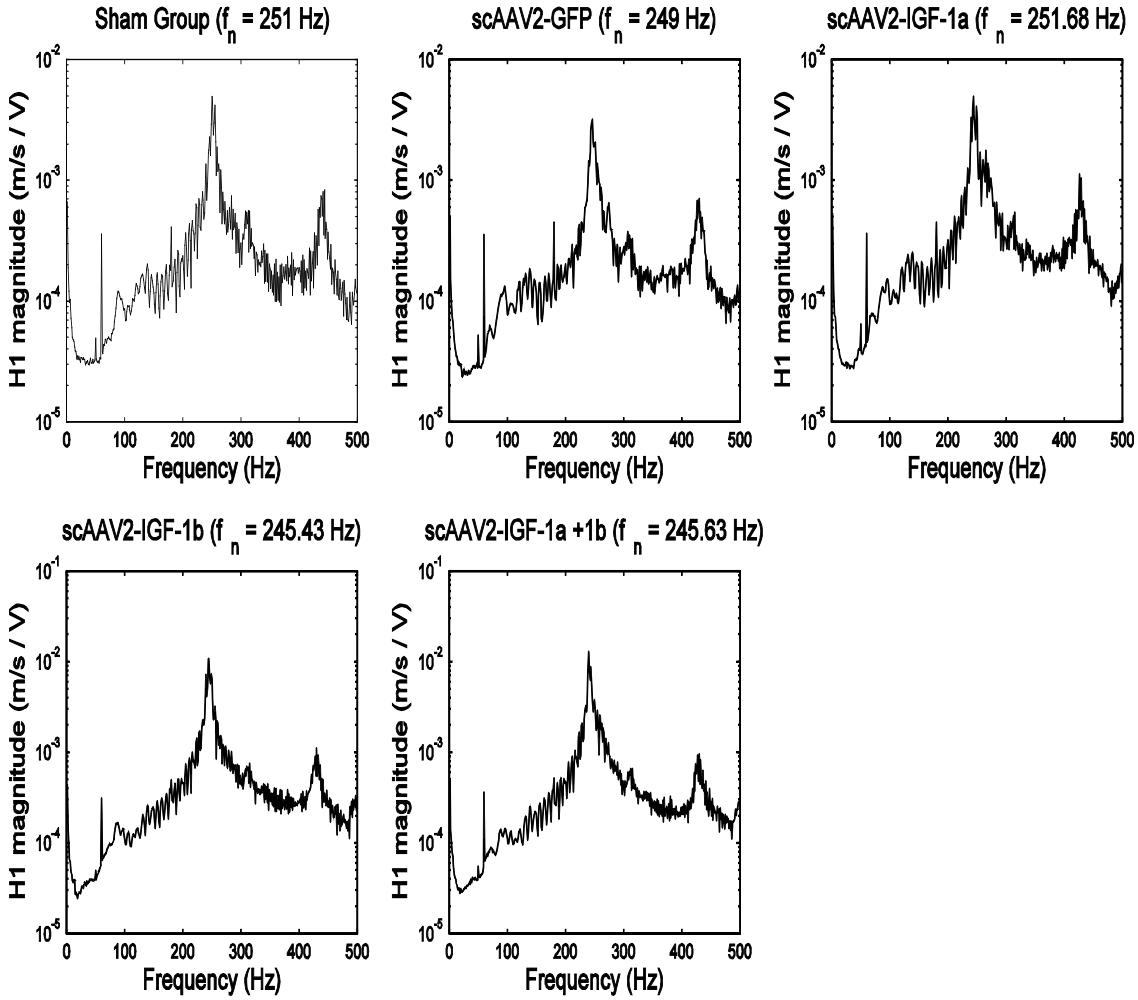

Figure 4. 6: Frequency Response Function (H1) of five treatment groups indicating natural frequency

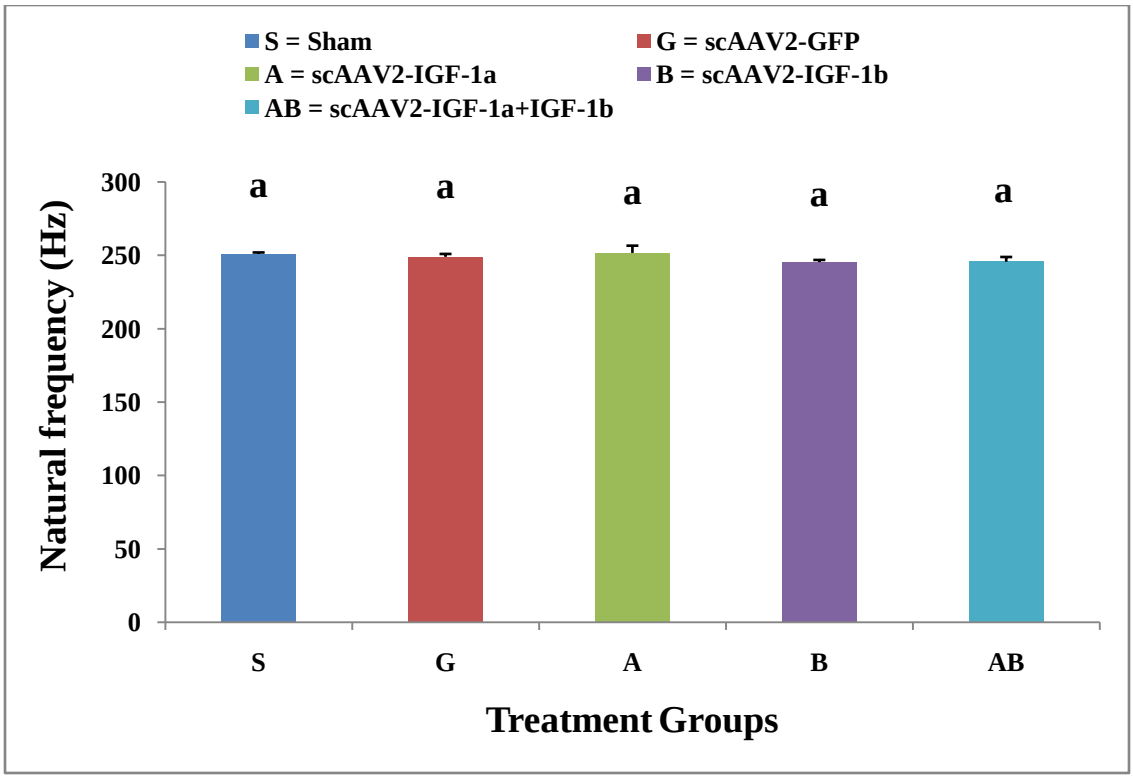

Figure 4. 7: Natural frequency (mean ± S.E.M). Natural frequencies of treatment groups are not significantly different (p > 0.05)

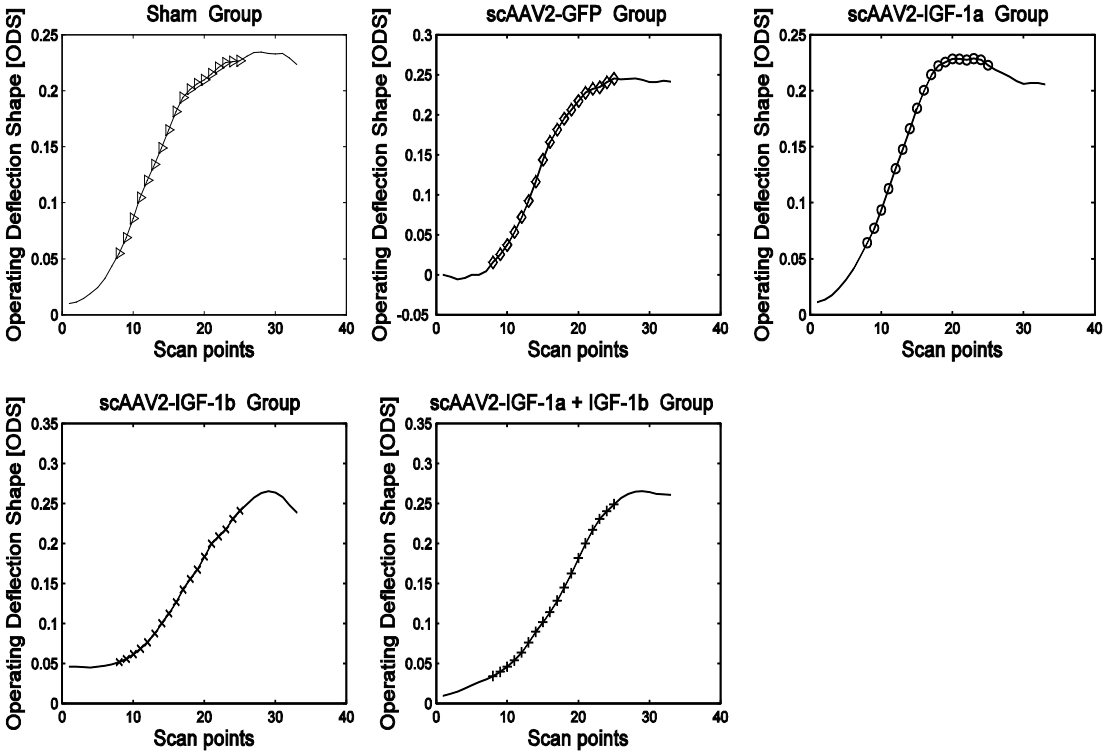

Figure 4. 8: Operating Deflection Shapes (ODS) of five treatment groups

Second mode frequencies are graphically presented in Figure 4.9. Sham group was significantly different from treatment groups scAAV2-GFP, scAAV2-IGF-1a, scAAV2-IGF-1b ($p = 0.014$, $p = 0.0058$ and $p = 0.0123$ respectively). Treatment group scAAV2-IGF-1a+IGF-1b trended to be significantly different from the sham group ($p = 0.0714$). First mode and second mode frequencies of each ligament of all groups are compared in Table 4.1 in sequence.

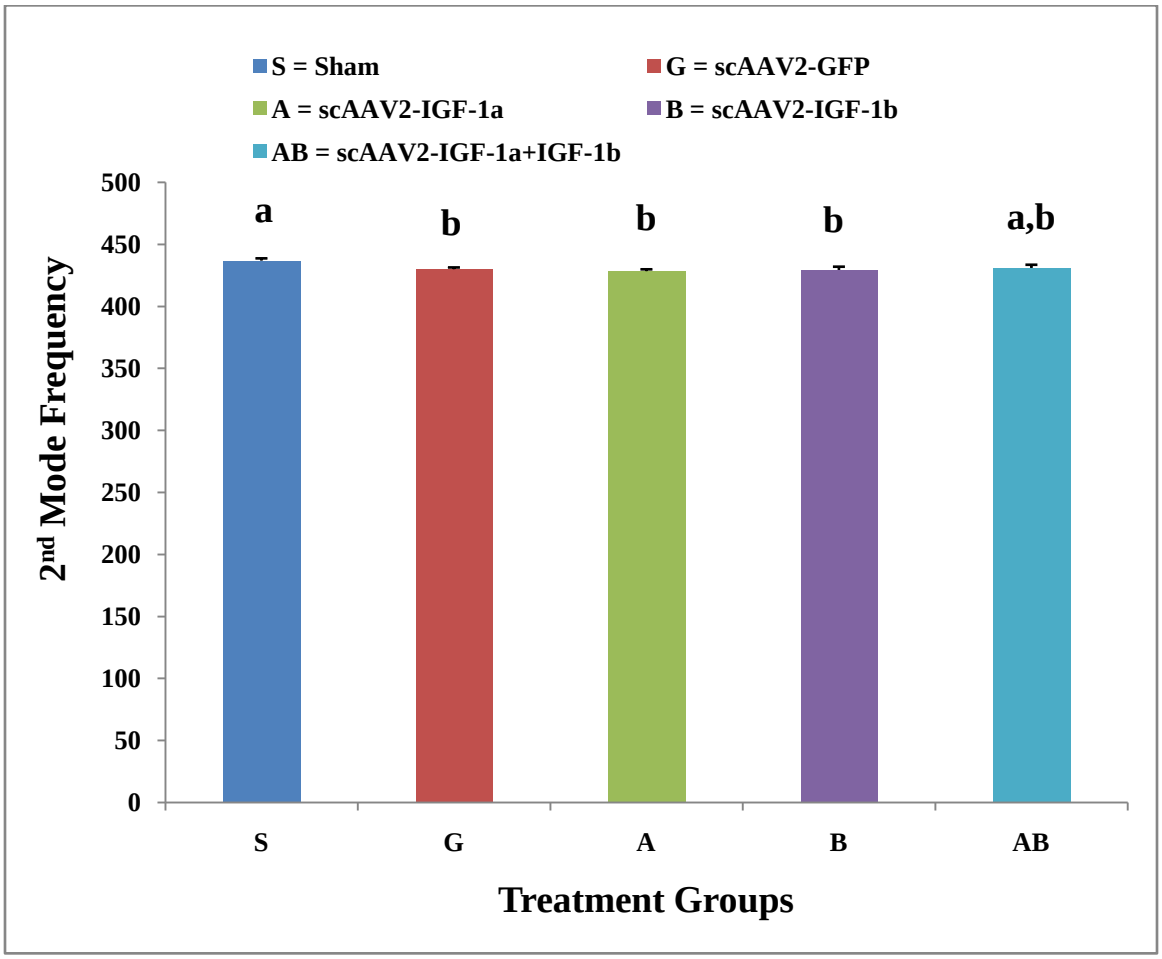

Figure 4. 9: Second Mode Frequency (mean ± S.E.M)

Table 4. 1: Comparison of 1st and 2nd mode frequencies

	Treatment 1 "S Group" (Hz)	Treatment 2 "G Group" (Hz)	Treatment 3 "A Group" (Hz)	Treatment 4 "B Group" (Hz)	Treatment 5 "AB Group" (Hz)
Lig – 1	250 – 430	257.5 – 428.75	268.8 – N/A	250 – N/A	250 – 430
Lig – 2	255 – 443.8	243.8 – N/A	243.75 – 426.3	243.8 – 430	240 – N/A
Lig – 3	250 – 438.8	246.3 – 430	248.75 – 432.5	245 – 427.5	240 – N/A
Lig – 4	250 – 436.3	246.3 – 435	242.5 – 428.75	240 – 423.75	243.75 – 427.5
Lig – 5	N/A – 435	248.8 – 430	241.3 – 426.25	248.75 – N/A	240 – N/A
Lig – 6	250 – 437.5	251.3 – 426.3	265 – N/A	245 – 436.3	260 – 436.25

4.2 DISCUSSIONS

Earlier research investigating MCL wound healing in rats indicate a maximum load on Sham control was in the range of 27 N (Mean±S.E.M) and ligaments treated with IGF displayed significant improvement in maximum load after three weeks of healing treatment (Provenzano et al. 2007). Our experimental tests are in agreement with these results as demonstrated by the maximum load to failure measures of Sham control group 23.32±1.55 N and the IGF-1b treated group which displayed the highest maximum load to failure of the treated ligaments. Ligaments treated with the IGF-1b isoform exhibited an increase in strength and toughness after 21 days of this gene therapy. Refer to Appendix B for values of all groups.

Figures 4.1 and 4.2 illustrate a wide change in stiffness for before and after relaxation in treated groups compared to the Sham group. Percentage of change in stiffness in control and treated ligaments is shown in Table 4.2.

Table 4. 2: Percentage of change in Stiffness of ligaments before and after relaxation

	Treatment 1 "S Group"	Treatment 2 "G Group"	Treatment 3 "A Group"	Treatment 4 "B Group"	Treatment 5 "AB Group"
Lig – 1	-	252.15	55.47	105.18	23.58
Lig – 2	33.48	147.50	-	217.52	97.56
Lig – 3	-17.84	81.17	65.84	245.45	-11.24
Lig – 4	-8.87	200.16	29.89	-	-
Lig – 5	-	104.41	-	143.99	168.05
Lig – 6	-9.27	112.76	68.35	80.31	72.22

We noticed the percentage change in stiffness in Sham control ligaments is less compared to the treated ligaments. Many factors play a key role in causing this effect. One among them may be structural orientation of fibers in ligaments. Ligaments are made of collagenous fibers whose structural orientation is nearly parallel. Structural orientation of fibers changes with the treatment performed on the ligament and the healing time associated with it. Each fiber in the ligament '*straightens out'* and to sustain a maximum load based on its orientation to the direction of principal load (Provenzano et al. 2007; Nordin and Frankel 2001). The load-displacement graphs for initial stiffness consists of toe-in region. A toe-in region is formed due to the removal of crimp pattern during deformation with the increase of stiffness. The presence of toe-in region is also a cause of decreased stiffness during initial elongation (Hurschler, Loitz-Ramage, and Vanderby 1997). Another biomechanical property causing changes in ligament stiffness

is the ligament viscoelastic properties. Viscoelastic properties of ligament are related to stress relaxation and creep. The percentage of stress relaxation of healing MCLs is significantly greater than sham control ligaments (Abramowitch et al. 2004). Treated healing ligaments are more viscoelastic, whereas sham control ligaments are more elastic. Therefore, a percentage change in the stiffness is high in healing treated ligaments.

The results of stiffness after relaxation of the MCLs shows that IGF-1b treated MCLs display a high stiffness value compared to GFP, IGF-1a, and IGF-1a-1b treated groups. The load to failure of IGF-1b treated MCLs was higher than other IGF treatment groups, IGF-1a and IGF-1a+1b, and also higher than the green fluorescent protein (GFP) treated group. The energy consumed to break the MCLs, which indicates toughness of ligament, was significantly higher in IGF-1b treatment group. Thus, the results obtained from this experiment demonstrate that MCLs treated with the IGF-1b isoform gene therapy are 1) stronger and tougher following three weeks of healing compared to control treatments, and 2) approached the strength and toughness of the intact Sham control ligaments, suggesting that IGF-1b gene therapy could potentially be a viable countermeasure to aid in and hasten dense fibrous connective tissue wound healing times.

Dynamic characteristics determined from our tests are natural frequencies and operating deflection shapes. Natural frequencies of the five treatments are not significantly different. These natural frequencies of five groups differ from each other with slight variations in the numerical values. All ligaments tested are small and area of ligament exposed to acoustic vibration makes it less likely to detect minute structural changes in the ligament. Our results are in agreement with experimental results published by Engelen et al, where the resonance frequency was shown to defer with changes in

mass and stiffness. Additional results also show that dissection of ligaments did not affect the resonance frequencies to a significant extent but the puncturing of the annulus reduced the natural frequency (Van Engelen et al. 2011). Revel et al. evaluated stress-strain curves and correlated them with the first vibration resonance frequency. Their data suggests that natural frequency increases as stress increases and the amplitude of vibration velocity does not affect natural frequency (Revel, Scalise, and Scalise 2003). Similarly, in our tests, we attempted to assess a best treatment among four treatment groups based on natural frequency, which demonstrates stiffness of the ligaments.

Operating deflection shapes of the five treatment groups indicates a first mode of the ligament at first natural frequency. The shape of ODS shows the movement of ligament under excitation. ODS are not significant from each other based on treatment regime, but we did notice some subtle differences in the ODS of five treatment groups. Our results can be compared with results displayed by Rusinek et al. His work concludes that the study of vibrations is necessary to detect behavior of inner ear ossicles. Damaged ossicles display an irregular behavior compared to normal ossicles (Rusinek et al. 2011). Similarly, operating deflection shapes of ligament demonstrate a sequence of motion of the ligament under excitation. Irregular behavior of deflection shape is used to detect damage of ligament. We did not notice any irregular deflection shapes in the ligaments from any of the treatment groups. This may be, in part, due to the very small knee ligament structure in the rat model.

In Figure 4.6, additional frequency response functions were noted and characterized. Specifically, a second mode in the process of formation was determined. We analyzed the second mode to obtain more information regarding the healing MCLs.

Early formation of a second mode is postulated to be associated with ligaments that possess decreased stiffness values compared to controls. The Sham group MLCs were stiffer compared to treated ligaments; however all ligaments in Sham group also displayed a second mode. A possible reason for this phenomenon could be explained by the architectural structure of Sham group, which is more robust compared to healing treated ligaments (Provenzano et al. 2007). When the second mode was compared between treated ligaments alone, we noticed that ligaments with high stiffness values did not display a second mode. Second mode frequencies pertaining to each ligament are presented in Table 4.1.

CHAPTER 5

CONCLUSIONS

This study was performed to assess static and dynamic biomechanical characteristics of healing MCLs treated with new gene therapies. A novel *de novo* mechanical test machine was constructed with a 'custom-built" load frame for static testing with an additional feature that included a laser vibrometer for dynamic testing. Dynamic testing helps in determining the integrity of ligaments by investigating their vibration characteristics associated with normal dense fibrous connective tissues.

Experiments were performed to test various MCL healing treatments among the four treatment groups (scAAV2-GFP, scAAV2-IGF-1a, scAAV2-IGF-1b, scAAV2-IGF-1b, scAAV2-IGF-1a + scAAV2-IGF-1b). According to the data derived from the static biomechanical testing, we suggest that scAAV2-IGF-1b could be a viable gene therapy treatment for injured ligaments. Reasons responsible for this conclusion are discussed below.

5.1 STATIC CHARACTERISTICS

In static testing, stiffness after the second elongation was significant in scAAV2-IGF-1a and scAAV2-IGF-1b when compared to scAAV2-IGF-1a+scAAV2-IGF-1b. In Load to failure scAAV2-IGF-1b was significantly different from scAAV2-GFP and scAAV2-IGF-1a+scAAV2-IGF-1b, but there was only a trend of scAAV2-IGF-1b treatment having a significant larger load to failure compared to scAAV2-IGF-1a treated group. This suggests that scAAV2-IGF-1b has maximum capacity to withstand load compared to other treatments in this study and approaches the maximum load to failure of the Sham control group. Results from energy consumed to disrupt the ligament show that

the scAAV2-IGF-1b treated group was significantly different from the other treatment groups: scAAV2-GFP, scAAV2-IGF-1a and scAAV2-IGF-1a + scAAV2-IGF-1b. scAAV2-IGF-1b was not significantly different from Sham control group. This suggests that the scAAV2-IGF-1b treatment aided in the ligament healing process by increasing the elastic storage energy compared to the control gene therapy treatments. Based on *de novo* MCL tissue static characteristics after 21 days of healing, we determine that scAAV2-IGF-1b gene therapy treatment yields the highest tissue strength and toughness following acute tissue regeneration of surgically transected MCLs.

5.2 DYNAMIC CHARACTERISTICS

Present work mainly focuses on assessing dynamic characteristics of ligament to determine resonance frequency and operating deflection shapes. To our knowledge, this is the first reported measurement of rat ligament biomechanical dynamic characteristics and also the first attempt at quantifying different mode shapes of injured ligaments in the process of healing.

Frequency response functions generated from the data obtained from the laser vibrometer delivered resonance frequencies. From our results we notice a first resonance phenomenon in all treatment groups in the range of 250 Hz. This is the first natural frequency of ligaments. The natural frequencies of each ligament treatment group are postulated to differ based on the stiffness of the ligament. The natural frequency was not significantly different between the five treatment groups. A second natural frequency was also detected in few of the ligaments from the treatment groups. We postulate that an early occurrence of a second natural frequency establishes that stiffness of ligament may be less than those ligaments that do not express a second natural frequency.

The operating deflection shape generated for the first natural frequency displayed the motion of the ligament during excitation. The mode shapes are similar with minimal distinction. The second mode frequency also played a role in determining stiffness of ligaments. All ligaments did not display a second natural frequency. The proper shape of the second mode at this frequency could not be determined due to limitations during testing.

The results of dynamic testing suggest that vibrations detected by the laser vibrometer demonstrated natural frequencies and operating deflection shapes of ligaments, but was not able to detect significant changes between the treatment groups possibly due to the miniscule size of rat ligaments being tested.

5.3 LIMITATIONS

The clamps that attached to “custom-built” load frame are in the vertical position. This causes difficulty in determining the alignment of the clamps. The final decision of clamp alignment was resolved through an “eye-ball test”.

During acoustic vibration testing, we obtained extraneous vibrations not related to the intrinsic vibrations associated with the ligament. The clamp attached to the load cell on one side of “custom-built” load frame displays a cantilever beam motion. We believe the origin of this vibration may originate within the clamp attachment. The vibrations of the clamp induced some vibration in tibia-ligament structure attached and mounted to the clamp. We considered these vibrations to be nominal as all ligaments during the experimental testing experience the same testing conditions.

The maximum speed of our picomotor (0.02 mm/sec) is very low compared to normal displacement velocities during biomechanical testing of soft tissues. The

displacement velocities of other picomotors generally employed during biomechanical testing are in range of 0.3mm/sec to 1.5 mm/sec.

The vibrometer scan head employed during our biomechanical testing is equipped with a macro (close-up) unit to measure vibrations in small specimens. This macro unit consists of various magnifying lenses. The use of the macro lenses blurs the video during real-time viewing making it hard to identify the ligament position. The magnifying lens minimizes the laser spot diameter, which is inversely proportional to accuracy.

CHAPTER 6

FUTURE DIRECTIONS

This research investigates IGF-I gene therapy in ligaments after 21 days of healing. Future research may consider longer healing periods to investigate other temporal biomechanical transitions that occur during other phases of ligament wound healing. Future gene therapy treatments could increase the proportion of IGF-1b transfected MCL fibroblast cells per fibrin glue delivery to each ligament in order to produce more IGF-1 protein.

The structure of a "custom-built" load frame could be modified to eliminate the cantilever beam motion of the clamp attached to load cell. Resolution of the load cell could be increased further to detect variations in load with greater sensitivity. A picomotor with a greater maximum speed of movement could also be employed to increase the speed of testing.

It would be optimal to create a vibration testing system located in a vibration-free environment in order to enhance the sensitivity of the acoustic vibration associated with ligaments without any other vibrational input from ancillary equipment or attachments. The model of laser vibrometer and revision of software used in this experiment were very basic and traditional versions which could be improved since newer technologies and computer codes have been developed since the purchase of our LDV and software. Newer laser vibrometer instruments contain better technology such as 1) a multi-point laser Vibrometer, which scans multiple points with single detector (Fu, Guo, and Phua 2011), and 2) an ultra high frequency Vibrometer that can analyze the vibrations in all types of microstructures. There are a few other features that can also be modified, such as

a clear real-time video magnifying lens add-on, excitation techniques using a function generator, and specifications to minimize the leakage of signals during the generation of frequency response functions. Lastly, sounds produced to create acoustic vibrations could be further optimized by using a high energy speaker in wide frequency ranges.

REFERENCES

Abramowitch, Steven D, Savio L Y Woo, Theodore D Clineff, and Richard E Debski. 2004. "An evaluation of the quasi-linear viscoelastic properties of the healing medial collateral ligament in a goat model." *Annals of Biomedical Engineering* 32 (3): 329-335.

Atkinson, K E. 1989. *An Introduction to Numerical Analysis*. *Journal of Computational and Applied Mathematics*. Vol. 125. Wiley. doi:10.1016/S0377-0427(00)00475-1.

Broesch, James D, Dag Stranneby, and William Walker. 2008. *Digital signal processing : instant access*. *Digital Signal Processing*. Newnes.

Castellini, P, L Scalise, and E P Tomasini. 1998. "Teeth mobility measurement: a laser vibrometry approach." *Journal of clinical laser medicine surgery* 16 (5): 269-272.

Christensen, A B, F Ammitzbøll, C Dyrbye, M Cornelissen, P Cornelissen, and G Van der Perre. 1986. "Assessment of tibial stiffness by vibration testing in situ--I. Identification of mode shapes in different supporting conditions." *Journal of biomechanics* 19 (1): 53-60.

Cornelissen, M, P Cornelissen, G Van Der Perre, A B Christensen, F Ammitzboll, and C Dyrbye. 1987. "Assessment of tibial stiffness by vibration testing in situ--III. Sensitivity of different modes and interpretation of vibration measurements." *Journal of Biomechanics* 20 (4): 333-342.

Cornelissen, P, M Cornelissen, G Van der Perre, a B Christensen, F Ammitzbøll, and C Dyrbye. 1986. "Assessment of tibial stiffness by vibration testing in situ--II. Influence of soft tissues, joints and fibula." *Journal of biomechanics* 19 (7): 551-61.

De Vita, Raffaella, and William S Slaughter. 2007. "A constitutive law for the failure behavior of medial collateral ligaments." *Biomechanics and Modeling in Mechanobiology* 6 (3): 189-197.

Eiber, Albrecht. 2008. "Mechanical problems in human hearing." *Studies in health technology and informatics* 133: 83-94.

Ewins, D J. 1984. *Modal Testing: Theory and Practice*. *Research Studies Press LTD.* Vol. 359. Research Studies Press.

———. 2001. *Modal Testing: Theory, Practice and Application*. Ed. Roberts. *book.* RESEARCH STUDIES PRESS LTD.

Foth, H J, C Huthoff, M Brenner, and S Färber. 1996. "Measuring the motions in the human middle ear by laser Doppler vibrometry." *Science* 25 (4-5): 289-301.

Fu, Y, M Guo, and P B Phua. 2011. “Multipoint laser Doppler vibrometry with single detector: principles, implementations, and signal analyses.” *Applied Optics* 50 (10): 1280-1288. doi:10.1364/AO.50.001280.

Gelse, K. 2003. “Collagens—structure, function, and biosynthesis.” *Advanced Drug Delivery Reviews* 55 (12): 1531-1546. doi:10.1016/j.addr.2003.08.002.

Gijssen, Yvo, Inger N Sierevelt, Jan G M Kooloos, and Leendert Blankevoort. 2004. “Stiffness of the healing medial collateral ligament of the mouse.” *Connective Tissue Research* 45 (3): 190-195.

Hansen, M, A Boesen, L Holm, A Flyvbjerg, H Langberg, and M Kjaer. 2012. “Local administration of insulin-like growth factor-I (IGF-I) stimulates tendon collagen synthesis in humans.” *Scandinavian journal of medicine & science in sports* (January 31). doi:10.1111/j.1600-0838.2011.01431.x.

Hart, D P, and L E Dahners. 1987. “Healing of the medial collateral ligament in rats. The effects of repair, motion, and secondary stabilizing ligaments.” *The Journal of Bone and Joint Surgery* 69 (8): 1194-1199.

He, Jimin, and Zhi-Fang Fu. 2001. *Modal Analysis*. *Modal Analysis*. Vol. 117. Butterworth-Heinemann.

Hurschler, C, B Loitz-Ramage, and R Vanderby. 1997. “A structurally based stress-stretch relationship for tendon and ligament.” *Journal of Biomechanical Engineering* 119 (4): 392-399.

Kurtz, C A, T G Loebig, D D Anderson, P J DeMeo, and P G Campbell. 1999. “Insulin-like growth factor I accelerates functional recovery from Achilles tendon injury in a rat model.” *The American Journal of Sports Medicine* 27 (3): 363-369.

Lechner, CT, and LE Dahners. 1991. “Healing of the medial collateral ligament in unstable rat knees.” *Am J Sports Med* 19: 508. doi:10.1177/036354659101900517.

Letson, A K, and L E Dahners. 1994. “The effect of combinations of growth factors on ligament healing.” *Clinical Orthopaedics and Related Research* (308): 207-212.

Martinez, Daniel A, and David Zimmerman. 2008. The impact of IGF-1 gene therapy to improve knee-ligament wound repair; NFL Charities Medical Grant Application. Houston.

Molloy, Timothy, Yao Wang, and George Murrell. 2003. “The roles of growth factors in tendon and ligament healing.” *Sports Medicine* 33 (5): 381-394.

Nishimori, Makoto, Tomoyuki Matsumoto, Shusuke Ota, Sebastian Kopf, Yutaka Mifune, Christopher Harner, Mitsuo Ochi, Freddie H Fu, and Johnny Huard. 2012.

"Role of angiogenesis after muscle derived stem cell transplantation in injured medial collateral ligament." *Journal of orthopaedic research : official publication of the Orthopaedic Research Society* 30 (4): 627-33.

Nordin, Margareta, and Victor H Frankel. 2001. *Basic biomechanics of the musculoskeletal system*. Ed. Butler. *New York*. Lippincott Williams & Wilkins.

Panjabi, M M, P Moy, T R Oxland, and J Cholewicki. 1999. "Subfailure injury affects the relaxation behavior of rabbit ACL." *Clinical Biomechanics* 14 (1): 24-31.

Paschos, Nikolaos K, Dimitrios Gartzonikas, Nektaria-Marianthi Barkoula, Constantina Moraiti, Alkis Paipetis, Theodore E Matikas, and Anastasios D Georgoulis. 2010. "Cadaveric study of anterior cruciate ligament failure patterns under uniaxial tension along the ligament." *Arthroscopy the journal of arthroscopic related surgery official publication of the Arthroscopy Association of North America and the International Arthroscopy Association* 26 (7): 957-967.

Provenzano, Paolo P, Adriana L Alejandro-Osorio, Kelley W Grorud, Daniel A Martinez, Arthur C Vailas, Richard E Grindeland, and Ray Vanderby. 2007. "Systemic administration of IGF-I enhances healing in collagenous extracellular matrices: evaluation of loaded and unloaded ligaments." *BMC Physiology* 7 (2): 2.

Provenzano, Paolo P, Daniel A Martinez, Richard E Grindeland, Kelley W Dwyer, Joanne Turner, Arthur C Vailas, and Ray Vanderby. 2003. "Hindlimb unloading alters ligament healing." *Journal of Applied Physiology* 94 (1): 314-324.

Rao, S. 2006. *Mechanical Vibrations*. *Notes*. Vol. 179. Prentice Hall. doi:10.1038/179504a0.

Revel, Gian Marco, Alessandro Scalise, and Lorenzo Scalise. 2003. "Measurement of stress–strain and vibrational properties of tendons." *Measurement Science and Technology* 14 (8): 1427-1436. doi:10.1088/0957-0233/14/8/332.

Rusinek, Rafał, Marcin Szymański, Jerzy Warmiński, Marek Zadrozniak, and Kamal Morshed. 2011. "Vibrations in the human middle ear." *Medical science monitor : international medical journal of experimental and clinical research* 17 (12): BR372-6.

Scalise, Lorenzo, Ilaria Ercoli, Paolo Marchionni, and Enrico Primo Tomasini. 2011. "Measurement of Respiration Rate in Preterm Infants by Laser Doppler Vibrometry." *Signal Processing*: 0-4.

Schwarz, Brian J, and Mark H Richardson. 1999. "Introduction to operating deflection shapes." *CSI Reliability Week Orlando FL*: 1-7.

Sim, Jae Hoon, Michael Lauxmann, Michail Chatzimichalis, Christof Röösli, Albrecht Eiber, and Alexander M Huber. 2010. “Errors in measurement of three-dimensional motions of the stapes using a laser Doppler vibrometer system.” *Hearing Research* 270 (1-2): 4-14.

Tashiro, Toshiyuki, Hisatada Hiraoka, Yasuko Ikeda, Toshiyuki Ohnuki, Ryuji Suzuki, Takahiro Ochi, Kozo Nakamura, and Naoshi Fukui. 2006. “Effect of GDF-5 on ligament healing.” *Journal of Orthopaedic Research* 24 (1): 71-79.

Vailas, A C, R F Zernicke, R E Grindeland, and K C Li. 1990. “Suspension effects on rat femur-medial collateral ligament-tibia unit.” *American Journal of Physiology* 258 (3 Pt 2): R724-R728.

Vanderby, R, A C Vailas, B K Graf, R J Thielke, M J Ulm, S S Kohles, and D N Kunz. 1990. “Acute modification of biomechanical properties of the bone-ligament insertion to rat limb unweighting.” *The FASEB journal official publication of the Federation of American Societies for Experimental Biology* 4 (8): 2499-2505.

Van Engelen, S J P M, A J Van Der Veen, A De Boer, M H M Ellenbroek, T H Smit, B J Van Royen, and J H Van Dieën. 2011. “The feasibility of modal testing for measurement of the dynamic characteristics of goat vertebral motion segments.” *Journal of Biomechanics* 44 (8): 1478-1483.

Wang, T-G, T-Y Hsiao, C-L Wang, and Y-W Shau. 2007. “Resonance frequency in patellar tendon.” *Scandinavian Journal of Medicine & Science in Sports* 17 (5): 535-538.

Warden, Stuart J, Leanne K Saxon, Alesha B Castillo, and Charles H Turner. 2006. “Knee ligament mechanical properties are not influenced by estrogen or its receptors.” *American Journal of Physiology - Endocrinology And Metabolism* 290 (5): E1034-E1040.

Whittemore, Kenneth R, Saumil N Merchant, Becky B Poon, and John J Rosowski. 2004. “A normative study of tympanic membrane motion in humans using a laser Doppler vibrometer (LDV).” *Hearing Research* 187 (1-2): 85-104.

Woo, S L, M A Gomez, M Inoue, and W H Akeson. 1987. “New experimental procedures to evaluate the biomechanical properties of healing canine medial collateral ligaments.” *Journal of Orthopaedic Research* 5 (3): 425-432.

Zhang, Guan-Ping, Tao Cu, Ai-Xia Wu, and Yong-Qi Li. 2007. “Establishment of mechanical middle ear model and the study of the acoustic characteristics of different ossicular prostheses.” *Zhonghua er bi yan hou tou jing wai ke za zhi Chinese journal of otorhinolaryngology head and neck surgery* 42 (2): 130-134.

Zhao, Ting Ting, Ming Jian Wang, Jian Ping Wu, and Yun Feng Song. 2011. "Application of LDV in Vibration Analysis of Satellite Solar Panel." *Applied Mechanics and Materials* 105-107 (September): 143-146.

APPENDIX A

Load – Displacement graphs indicating stiffness after initial elongation of all treatment groups is shown in Figure A.1. Initial Stiffness corresponding to each ligament in all five treatment groups after 1st elongation is shown in Table A.1. In all tables S group = Sham Group, G group = scAAV2-GHP group, A group = scAAv20IGF-1a group, B group = scAAV2-IGF-1b and AB group = scAAV2-IGF-1a+IGF-1b.

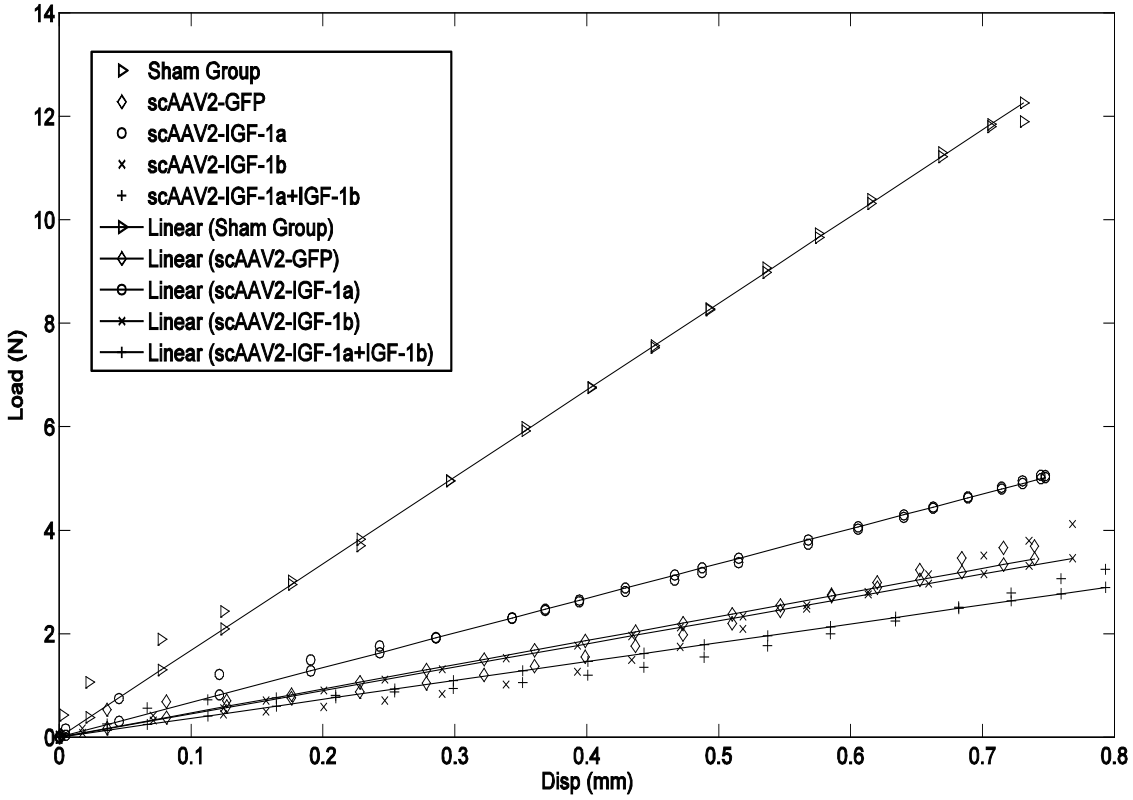

Figure A.1: Stiffness of five treatment groups after initial elongation

Table A.1: Stiffness of ligaments after initial elongation

	Treatment 1 "S Group" (N/mm)	Treatment 2 "G Group" (N/mm)	Treatment 3 "A Group" (N/mm)	Treatment 4 "B Group" (N/mm)	Treatment 5 "AB Group" (N/mm)
Lig – 1	-	2.29	6.85	7.95	7.22
Lig – 2	12.01	4.23	-	2.93	1.58
Lig – 3	19.48	4.98	7.85	2.59	1.44
Lig – 4	17.05	6.14	6.41	-	-
Lig – 5	-	5.81	-	5.54	1.36
Lig – 6	18.64	4.08	5.69	7.36	6.98
Mean $\pm$ SEM	16.79$\pm$1.67	4.59$\pm$0.57	6.70$\pm$0.45	5.27$\pm$1.10	3.71$\pm$1.38

APPENDIX B

Load-Displacement graphs after relaxation displaying maximum load to failure of each group are presented here.

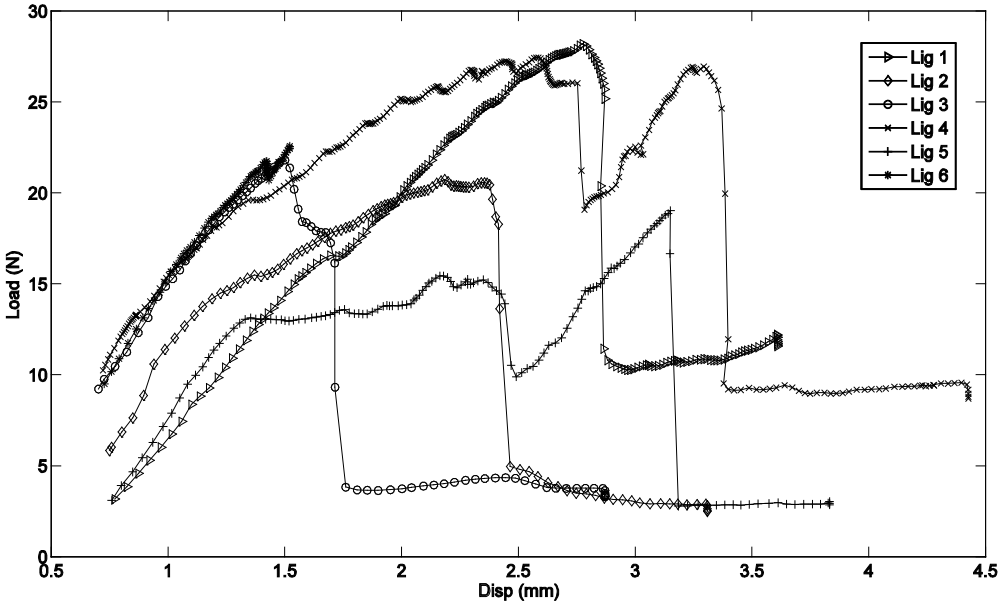

Figure B.1: Load vs. Displacement graph displaying maximum load to failure of Sham Group

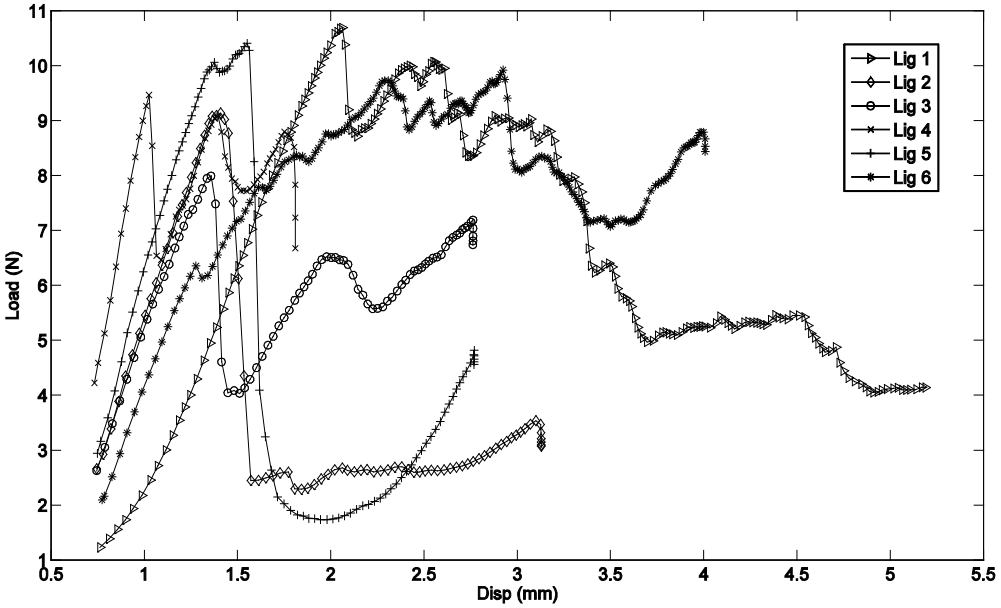

Figure B.2: Load vs. Displacement graph displaying maximum load to failure of scAAV2-GFP Group

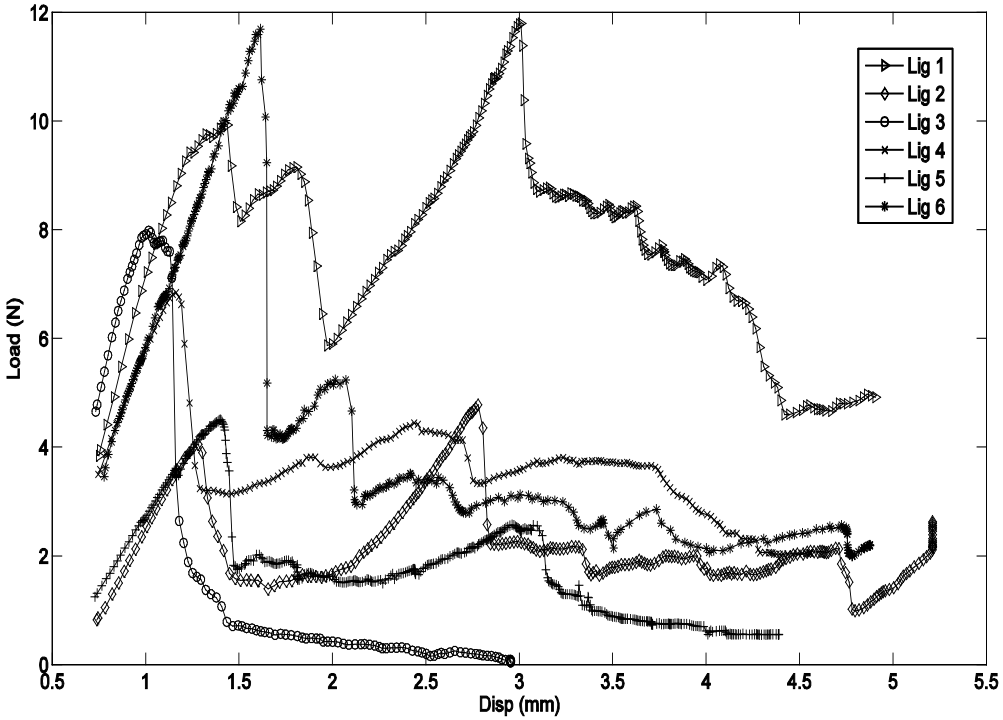

Figure B.3: Load vs. Displacement graph displaying maximum load to failure of scAAV2-IGF-1a Group

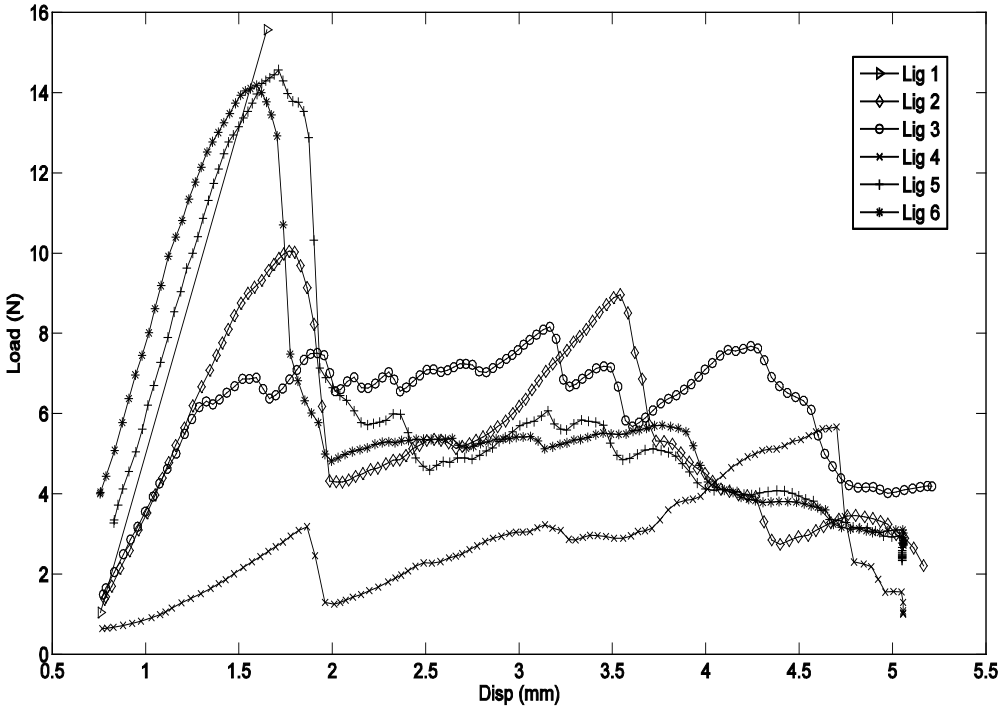

Figure B.4: Load vs. Displacement graph displaying maximum load to failure of scAAV2-IGF-1b Group

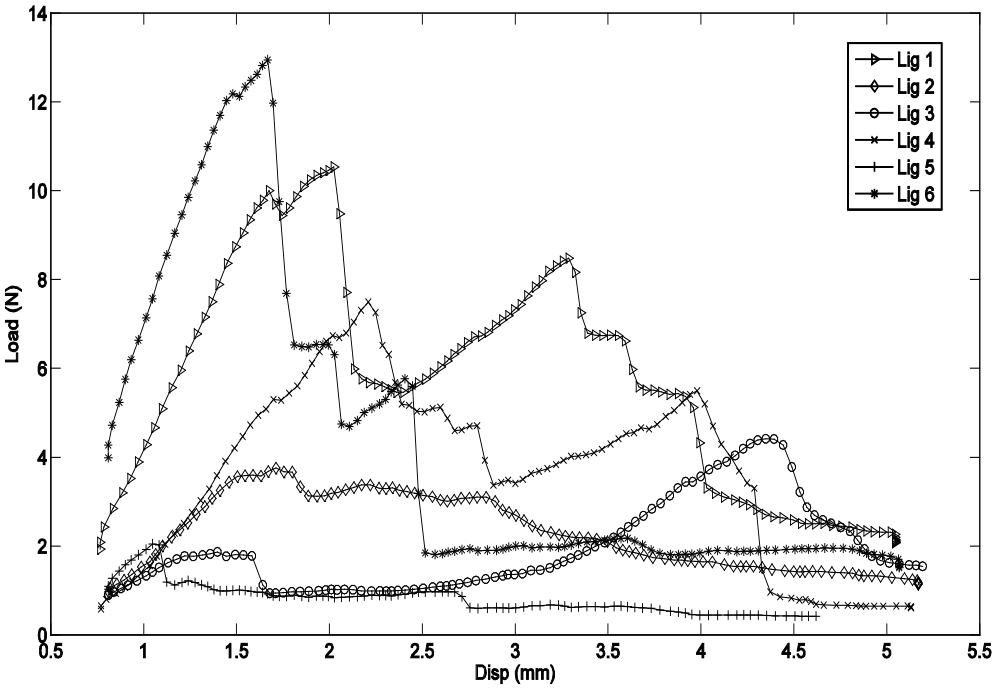

Figure B.5: Load vs. Displacement graph displaying maximum load to failure of scAAV2-IGF-1a+IGF-1b Group

Table B.1: Maximum load to failure of each ligament

	Treatment 1 "S Group" (N)	Treatment 2 "G Group" (N)	Treatment 3 "A Group" (N)	Treatment 4 "B Group" (N)	Treatment 5 "AB Group" (N)
Lig – 1	28.20	10.69	11.78	15.57	10.53
Lig – 2	20.75	9.14	-	10.05	3.76
Lig – 3	21.82	7.99	7.98	-	4.41
Lig – 4	27.47	9.47	6.84	-	7.49
Lig – 5	19.06	10.41	-	14.57	-
Lig – 6	22.60	9.92	11.69	14.18	12.95
Mean $\pm$ SEM	23.32$\pm$1.55	9.60$\pm$0.40	9.58$\pm$1.27	13.59$\pm$1.22	7.83$\pm$1.76

APPENDIX C

Stiffness of ligaments of each group after relaxation till maximum load to failure is calculated and presented here.

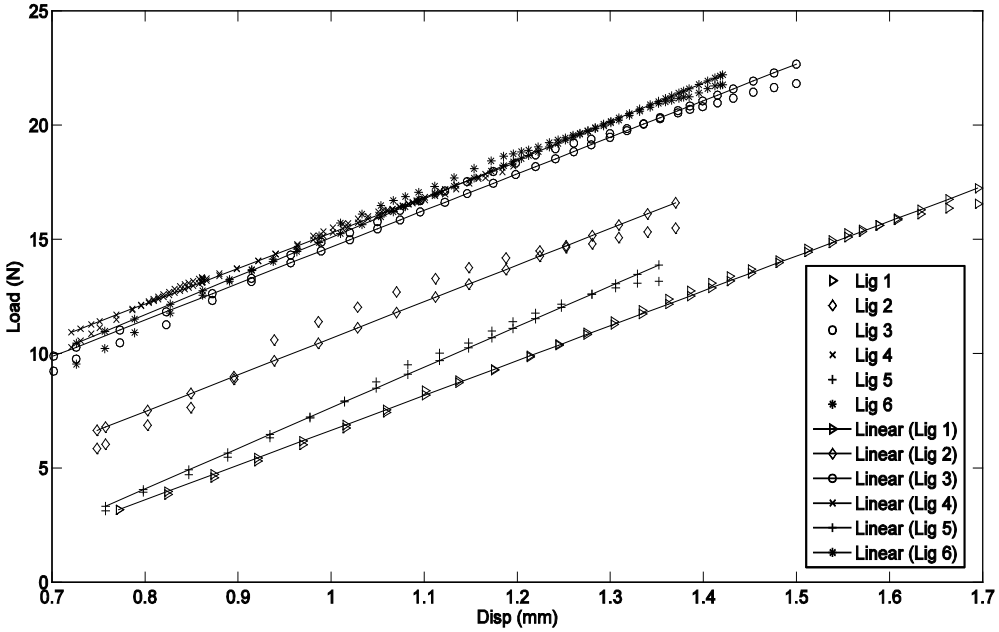

Figure C.1: Load vs. Displacement graph denoting stiffness of Sham Group

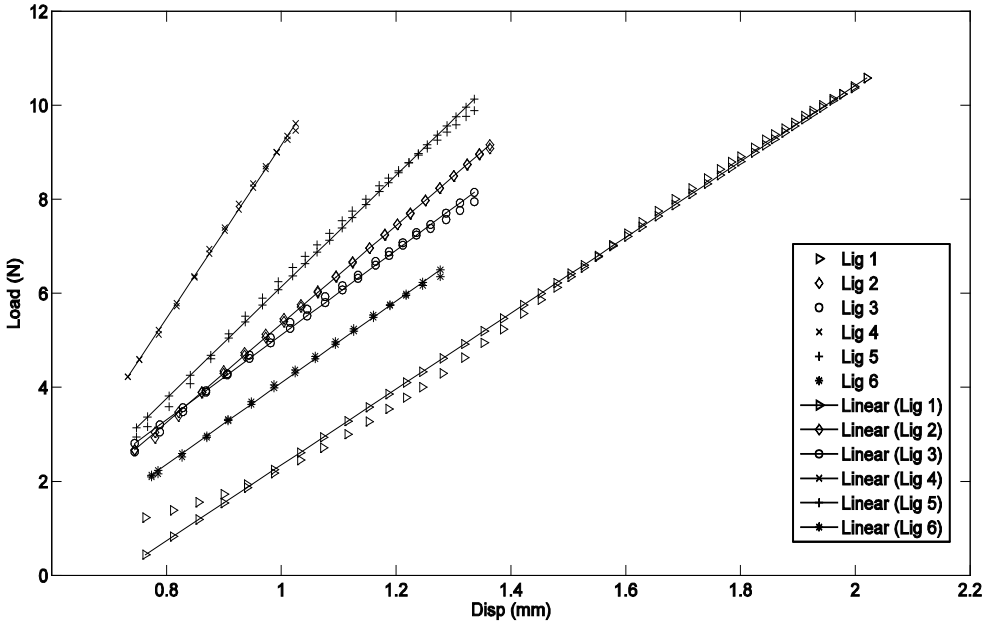

Figure C.2: Load vs. Displacement graph denoting stiffness of scAAV2-GFP Group

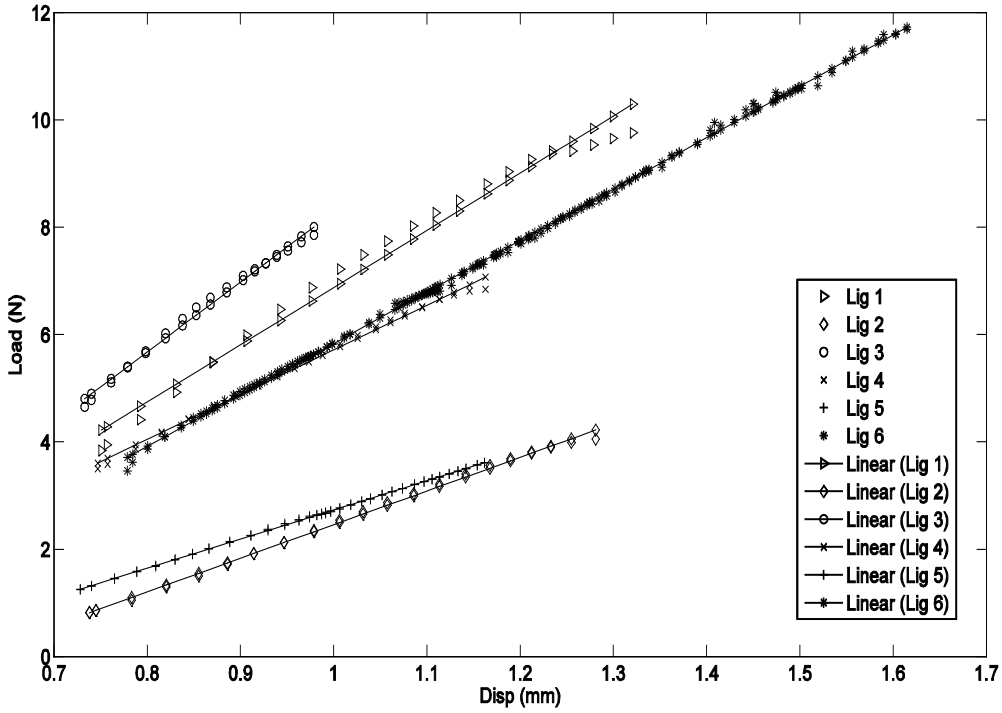

Figure C.3: Load vs. Displacement graph denoting stiffness of scAAv2-IGF-1a Group

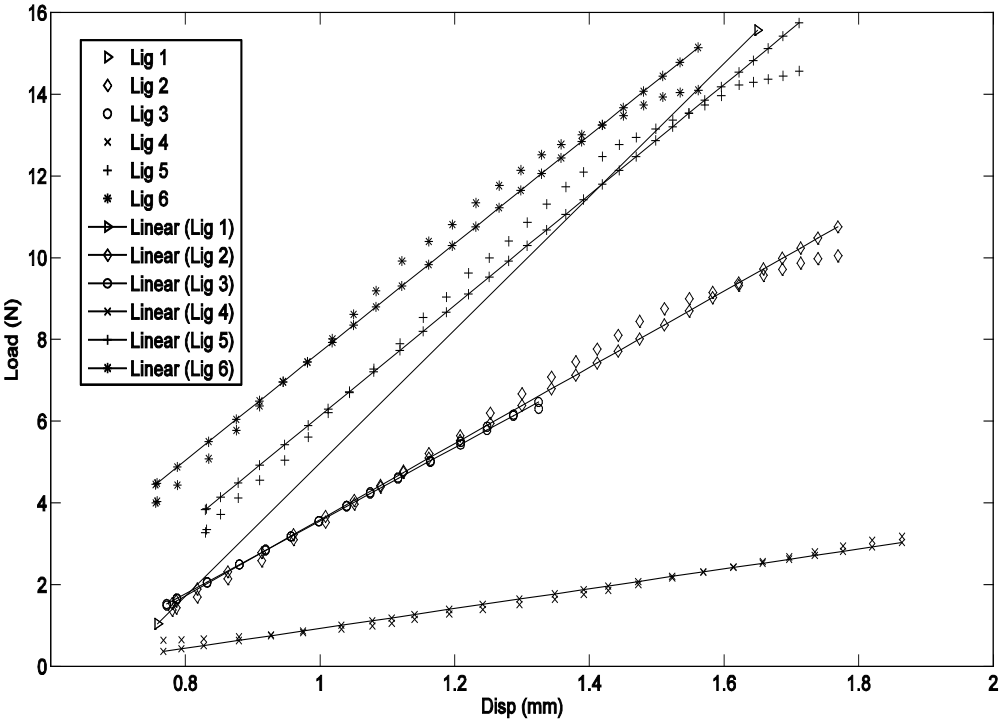

Figure C.4: Load vs. Displacement graph denoting stiffness of scAAv2-IGF-1b Group

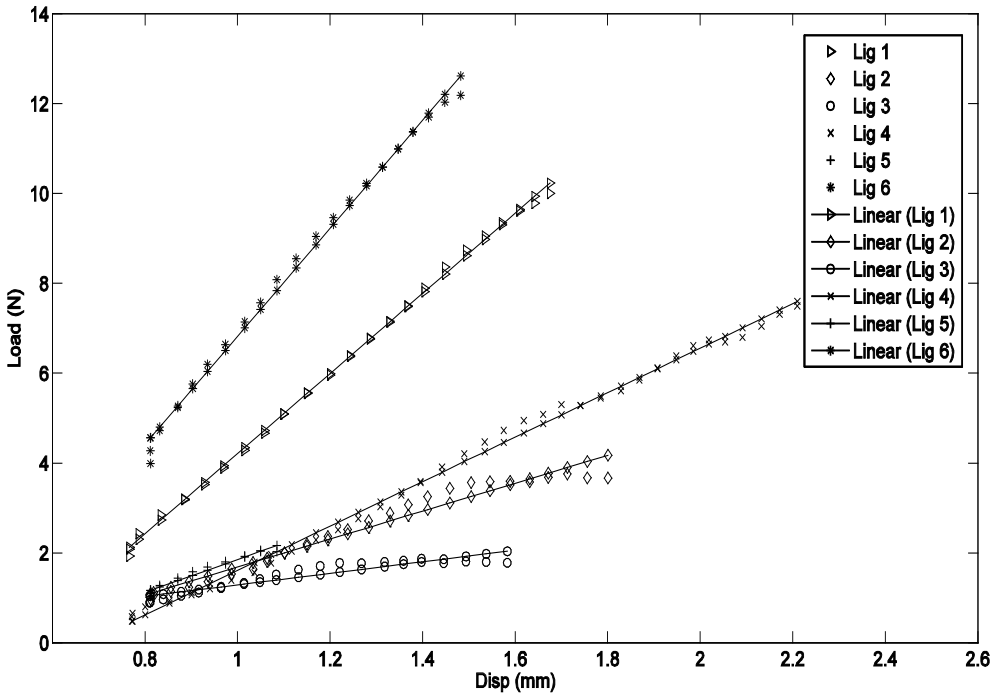

Figure C.5: Load vs. Displacement graph denoting stiffness of Sham Group

Table C.1: Stiffness of ligaments after relaxation and 2nd elongation.

	Treatment 1 "S Group" (N/mm)	Treatment 2 "G Group" (N/mm)	Treatment 3 "A Group" (N/mm)	Treatment 4 "B Group" (N/mm)	Treatment 5 "AB Group" (N/mm)
Lig – 1	15.25	8.07	10.66	16.30	8.92
Lig – 2	16.03	10.48	-	9.32	3.11
Lig – 3	16.01	9.02	13.03	8.95	1.28
Lig – 4	15.54	18.43	8.33	-	4.95
Lig – 5	17.76	11.87	-	13.51	3.65
Lig – 6	16.91	8.68	9.59	13.26	12.01
Mean ± SEM	16.25±0.37	11.09±1.57	10.40±0.99	12.27±1.39	5.65±1.65

Table C.2: Work to failure (Energy necessary to break the ligament)

	Treatment 1 "S Group" (N-mm)	Treatment 2 "G Group" (N-mm)	Treatment 3 "A Group" (N-mm)	Treatment 4 "B Group" (N-mm)	Treatment 5 "AB Group" (N-mm)
Lig – 1	9.41	-	-	7.40	5.63
Lig – 2	7.31	3.66	1.37	6.11	2.62
Lig – 3	12.99	3.25	1.58	-	1.20
Lig – 4	6.94	2.03	2.22	-	5.79
Lig – 5	5.13	3.91	1.06	8.69	-
Lig – 6	11.35	2.18	-	7.95	5.80
Mean $\pm$ SEM	8.86$\pm$1.20	3.65$\pm$0.88	1.56$\pm$0.25	7.54$\pm$0.54	4.21$\pm$0.96

APPENDIX D

Table D.1: Natural Frequencies of each ligament five treatment groups measured during relaxation period

	Treatment 1 "S Group" (Hz)	Treatment 2 "G Group" (Hz)	Treatment 3 "A Group" (Hz)	Treatment 4 "B Group" (Hz)	Treatment 5 "AB Group" (Hz)
Lig – 1	250	257.5	268.8	250	250
Lig – 2	255	243.8	243.75	243.8	240
Lig – 3	250	246.3	248.75	245	240
Lig – 4	250	246.3	242.5	240	243.75
Lig – 5	-	248.8	241.3	248.75	240
Lig – 6	250	251.3	265	245	260
Mean $\pm$ SEM	251$\pm$1	249$\pm$1.99	251.68$\pm$4.95	245.43$\pm$1.47	245.63$\pm$3.29